DYNAMICS OF MULTICELLULAR AGGREGATION AND DISAGGREGATION:

IMPLICATIONS FOR TISSUE ENGINEERING AND CANCER METASTASIS

Thesis by

Melissa Davis Pope

In partial fulfillment of the requirements

For the degree of

Doctor of Philosophy

CALIFORNIA INSTITUTE OF TECHNOLOGY

Pasadena, CA

2010

(Defended May 10, 2010)

ACKNOWLEDGEMENTS

thesis – I think he'll be as pleased as me on the day I turn it in. Because of sharing these past years with Brian, life outside of Caltech has been happy, fun and exciting. In fact, we recently welcomed a new member into our family. Our son, Jackson, with his boundless energy, great curiosity and bright smile has brought such joy into our lives. I am blessed to be Brian's wife and Jackson's mommy and I love them with all my heart.

I am deeply indebted to my wonderful parents, Ian Davis and Pamela Davis Kotzin, who have been endlessly enthusiastic through all of my endeavors. It is due to their love and encouragement that I have found much happiness and fulfillment in my life. A special thank you to my mom for spending many of her days caring for Jackson while I finished my thesis. And a special thank you to my dad for getting me started on the whole "science" thing in the first place – I think you would have gotten a kick out of "Melissa, Ph.D."

I am also grateful to my mother-in-law, Judith Pope, who made several trips from Pennsylvania to live with us and care for Jackson while I finished my thesis. She cared for Jackson (and for Brian and me) with much energy and love. Much thanks too to my father-in-law, Robert Pope, for parting with his beloved Judy for so many weeks.

Finally, I have been blessed with many wonderful friends who have made this stage of my life rich with love and laughter: Barbara Ngo, Katie Brenner, Katie Galloway, Stacey Maskarinec, Julia Chen, the girls (now the mommies!) of Warehouse, Shelly Tzlil, Roseanna Zia and Harmony Gates.

ABSTRACT

DYNAMICS OF MULTICELLULAR AGGREGATION AND DISAGGREGATION:

IMPLICATIONS FOR TISSUE ENGINEERING AND CANCER METASTASIS

May 2010

Melissa Davis Pope

B.S., Chemical Engineering, University of California, Irvine

Ph.D., Bioengineering, California Institute of Technology

Epithelial tissues play an important physiological role. Tightly cohesive epithelial sheets form protective barriers that line organs, and in addition, fold into a wide variety of complex 3D architectures with specialized functions. A key facet of tissue morphogenesis involves the aggregation of similar cells into cohesive groups. Here, we have analyzed the dynamics of aggregation using quantitative imaging techniques (Chapter II). We show that multicellular aggregation dynamics adhere to a transport-reaction model that is broadly appreciated for physicochemical systems. This model of aggregation dynamics differs from the classical equilibrium paradigm of cell aggregation based on differential adhesivity of cells to neighboring cells versus the underlying substratum. Our findings reveal a previously unrecognized role for cell motility during developmental aggregation processes and provide design principles for promoting cell aggregation dynamics in contexts such as tissue engineering that are distinct from the currently accepted paradigm.

Multicellular aggregation is reversible. In fact, the break-up of multicellular clusters ("cell scatter") is not only important for developmental processes, but also contributes to metastasis. However, current molecular genetics studies of cell scatter are predominantly qualitative and do not provide a quantitative assessment of the relative strengths of molecular signals in inducing cell scatter. By developing and implementing an automated image processing algorithm, we quantify two aspects of cell scatter – the breakdown of cell-cell adhesions and the dispersion of detached cells – in mammary epithelial cells treated with different combinations of biochemical cues (Chapter III). We demonstrate that our metrics of cell scatter identify the effects of individual cues and detect synergies between them. We envision that this approach will be useful for mapping the relative potencies of regulators of cell scatter and may guide therapeutic strategies.

Multicellular processes such as aggregation and scatter involve molecular-level changes within cell-cell adhesions. To complement imaging-based strategies at the cellular and multicellular levels, we developed a quantitative microtiter assay for examining the expression of cell-cell adhesion proteins and associations between them (Chapter IV). Using two case studies related to cancer biology, we demonstrate that our assay provides a more detailed quantitative picture of molecular changes within epithelial adhesive structures, which can provide added insight into the regulation of morphogenetic events.

TABLE OF CONTENTS

Chapter I. Introduction

Chapter II. Short-lived cell-cell interactions foster transport-limited cell aggregation: biphasic dependence of aggregation dynamics on substratum adhesivity

Chapter III. Automated Quantitative Analysis of Epithelial Cell Scatter

Chapter IV. A microtiter assay for quantifying protein-protein interactions associated with cell-cell adhesion

LIST OF TABLES

LIST OF FIGURES

Chapter I. INTRODUCTION

1. Introduction

The assembly of migratory cells into a cohesive group is a key facet of embryonic tissue development. Multicellular condensation occurs in the initial stages of chondrogenesis (cartilage formation), for example, and is believed to be a prerequisite for chondrogenic differentiation.[1] In addition, migrating neural crest cells are observed to condense into sub-populations en route to distant embryonic sites. This is thought to facilitate the immobilization of these cells to form solid tissues.[2]

In addition to multicellular aggregation, the dissociation of single cells from condensed tissue can also play a key role in tissue development. Kidney development, for example, is characterized by repeated cycles of condensation and dissociation.[3-5] In addition, delamination of endothelial cells from the embryonic atrioventricular canal gives rise to a cell population that eventually forms the heart valves.[6] Cellular dissociation also plays a role in tumorigenesis. In this context, metastatic cells delaminate from the tumor mass and migrate to secondary sites, thereby initiating the lethal phase of cancer progression.[7]

At the molecular level, condensation and dissociation events are often associated with a mesenchymal-epithelial transition or an epithelial-mesenchymal transition (EMT), respectively.[8] These transitions are triggered by extracellular activators and

characterized by the gain (MET) or loss (EMT) of epithelial characteristics such as the expression of cell-cell adhesion receptors. Condensation and dissociation also involve cellular processes, such as cell-cell adhesion, cell-matrix adhesion and cell migration on the extracellular matrix.

2. Adherens junctions mediate strong cell-cell adhesion

In epithelial tissues, E-cadherin-containing adherens junctions are important mediators of cell-cell adhesion.[9] E-cadherin is a transmembrane protein, the extracellular domain of which homotypically binds E-cadherin molecules on adjacent cells.[10] The intracellular tail connects to the actin cytoskeleton via protein:protein interactions involving α-catenin, β-catenin, vinculin and many other proteins. In this manner, adherens junctions link the actin cytoskeleton of contacting cells, creating an "actin belt" that imparts structural strength to a multicellular aggregate (Figure I-1).
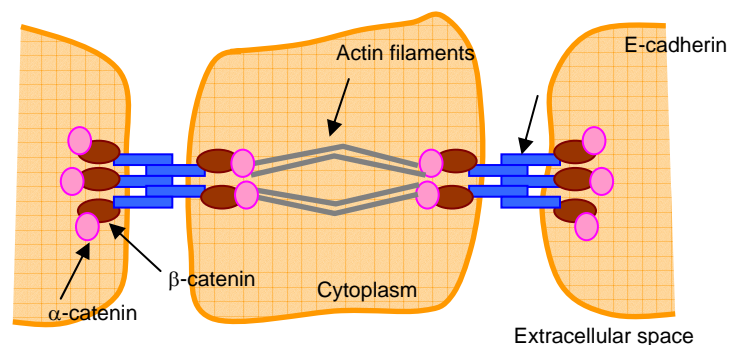
Figure I-1. Generalized structure of adherens junctions.
E-cadherin molecules span the plasma membrane to bind E-cadherin molecules on neighboring cells. E-cadherin's cytoplasmic tail interacts with β-catenin and α-catenin, forming a connection to the actin cytoskeleton.

3. Focal adhesions assemble at sites of cell-matrix adhesion

Cells use many adhesion receptors to attach to the extracellular matrix, the most prominent being the integrin family of transmembrane receptors. Integrin extracellular domains recognize a protein component of the extracellular matrix, while the intracellular domain interacts with numerous anchor proteins to form signaling-rich complexes called focal adhesions.[11] These anchor proteins, which include talin, α-actinin and vinculin, tether integrins to the actin cytoskeleton and enable cell-generated contractile forces to be transmitted onto the underlying substratum, generating the driving force needed for cell migration (Figure I-2).[12]
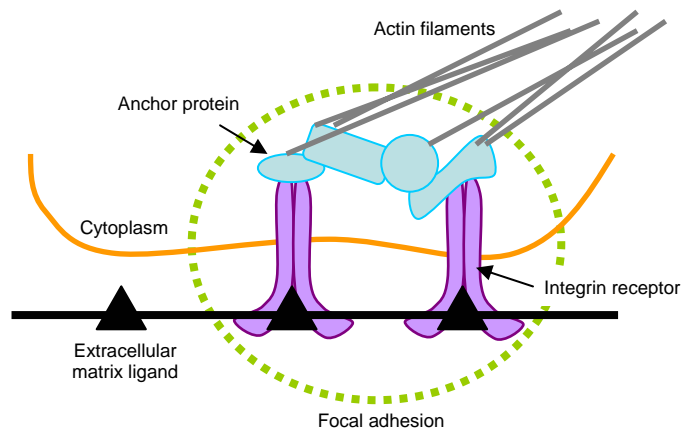
Figure I-2. Generalized structure of focal adhesions.

Integrin transmembrane receptors bind to extracellular matrix ligands. Integrin cytoplasmic tails bind to multiple anchor proteins, which tether integrins to the actin cytoskeleton to mediate strong cell-substratum adhesion.

4. Cell migration on the extracellular matrix

Cell migration is a cyclic process. A cell first extends membrane protrusions – spike-like filopodia and broad lamellopodia – in the direction of movement. These

protrusions are driven by actin polymerization and stabilized by the assembly of focal adhesions beneath them. Focal adhesions provide the traction necessary to translocate the cell body forward, and are subsequently disassembled at the cell rear to allow the trailing edge to detach from the substratum (Figure I-3).[12] Because migrating cells must be able to exert traction yet readily detach, cell speed exhibits a biphasic dependence on substratum adhesivity – a weakly adhesive substratum facilitates little traction while a strongly adhesive substratum inhibits detachment.[13]

Actin filaments

New adhesions

(B) Translocation

Focal adhesions

(C) Rear retraction

(A) Protrusion and
adhesion formation
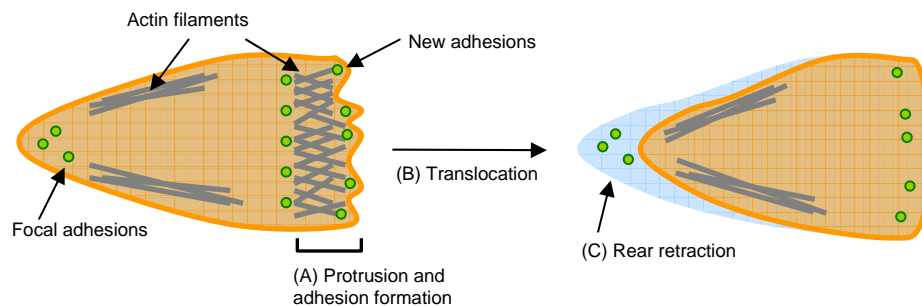
Figure I-3. Steps in cell migration.

(A) Actin polymerization drives membrane protrusions at the leading end of the cell, where new cell-substratum adhesions are formed. (B) These newly-formed adhesions provide the traction necessary to translocate the cell body forward. (C) Adhesions are disassembled at the trailing end of the cell to allow cell detachment from the substratum. Adapted from Ridley et al. *Science* (2003).

5. Current results

To better understand the roles of cell-cell interactions, cell-matrix adhesions and cell migration in condensation and dissociation, we utilize *in vitro* aggregation and scatter assays that mimic these *in vivo* phenomena. Epithelial cells cultured on adhesive substrata self-assemble into 2D multicellular clusters ("aggregation"). In response to

extracellular cues, these cell clusters dissociate and individual cells disperse ("scatter"). Aggregation and scatter are widely used model systems in which to study condensation and dissociation events. In fact, the current understanding of the complex biochemical network regulating EMT comes largely from studies of cell scatter.[8]

The classical paradigm describing multicellular aggregation asserts that the equilibrium state of aggregation is determined by differential cell adhesivity to neighboring cells versus the underlying substratum.[14-16] Because organ formation is a multi-step process, *in vivo* aggregation events must occur within specific time constraints. Therefore, aggregation dynamics are likely to be important. We assert that because cells must first "find" a neighbor (a transport step) before forming cell-cell contacts, aggregation dynamics may follow a transport-reaction model ascribed widely to physiochemical systems.[17, 18] In Chapter II, we present quantitative studies of aggregation dynamics that probe this possibility. Using timelapse microscopy, we tracked collisions between migrating cell pairs and quantified the lifetimes of cell-cell interactions ($t_{adhesion}$). Based on the initial density of seeded cells and quantitative measurements of cell speed, we also determined the mean time between cell-cell collisions ($t_{motility}$). We find that $t_{motility}$ is greater than $t_{adhesion}$ across a range of adhesive substrata, suggesting aggregate assembly to be transport-limited. Quantitative measurements of aggregate size confirm this to be the case: aggregate size exhibits a biphasic dependence on substratum adhesivity, which mimics the biphasic trend observed for cell speed. These results are consistent with a two-step physiochemical model for multicellular aggregation dynamics and highlight a previously unrecognized role for

cellular motility in aggregation dynamics. Our study provides insight into a developmental phenomenon and design principles useful for facilitating multicellular aggregation in tissue engineering contexts.

Because of the physiological and clinical significance of dissociation events, much effort has been made to identify the molecular signals that control cell scatter. Advancements are being made in cataloging the signaling pathways involved; however because current studies of cell scatter are largely qualitative, an emerging challenge is to understand the quantitative contributions of these signals and any coupling between them. In Chapter III, we have therefore developed novel quantitative metrics to systematically characterize cell scatter. Our metrics capture two aspects of scatter – the break-down of cell-cell contacts and cellular dispersion. In mammary epithelial cells treated with stimulatory cocktails containing epidermal growth factor (EGF), we demonstrate that our metrics delineate the effects of individual molecular signals and detect synergies between them. To facilitate the rapid extraction of our metrics from fluorescence images of scattering cells, we have also developed automated image processing techniques using MATLAB. We envision that these metrics coupled with our automated image processing techniques will facilitate quantitative mapping of the biochemical cues governing scatter as well as high throughput screening of cancer therapeutics.

Multicellular processes such as aggregation and scatter involve changes to the expression levels of and interactions between cell-cell adhesion proteins. The association of E-cadherin with intracellular binding partner β-catenin, for example, is essential for

the proper function of epithelial adherens junctions and is an attractive molecular readout of their integrity. To complement our imaging-based studies at the cellular and multicellular levels, we have developed a quantitative microtiter assay for determining the amount β-catenin bound to E-cadherin in cultured cells (Chapter IV). In two case studies closely related to cancer cell biology, we demonstrate that our assay can provide a more detailed picture of molecular dynamics within adherens junctions, which will provide added insight into aggregation and scatter.

Taken together, these studies provide novel insights into the regulation of aggregation and scatter as well as methodologies useful for both future studies and biomedical applications.

6. References

1. Oberlender SA, Tuan RS. Expression and functional involvement of N-cadherin in embryonic limb chondrogenesis. Development (Cambridge, England) 1994; 120:177-87.

2. Nakagawa S, Takeichi M. Neural crest cell-cell adhesion controlled by sequential and subpopulation-specific expression of novel cadherins. Development (Cambridge, England) 1995; 121:1321-32.

3. Davies JA. Mesenchyme to epithelium transition during development of the mammalian kidney tubule. Acta anatomica 1996; 156:187-201.

4. Dressler G. Tubulogenesis in the developing mammalian kidney. Trends in cell biology 2002; 12:390-5.

5. Hay ED, Zuk A. Transformations between epithelium and mesenchyme: normal, pathological, and experimentally induced. Am J Kidney Dis 1995; 26:678-90.

6. Mercado-Pimentel ME, Runyan RB. Multiple transforming growth factor-beta isoforms and receptors function during epithelial-mesenchymal cell transformation in the embryonic heart. Cells, tissues, organs 2007; 185:146-56.

7. Thiery JP. Epithelial-mesenchymal transitions in tumour progression. Nat Rev Cancer 2002; 2:442-54.

8. Thiery JP, Sleeman JP. Complex networks orchestrate epithelial-mesenchymal transitions. Nature reviews 2006; 7:131-42.

9. Gumbiner BM. Cell adhesion: the molecular basis of tissue architecture and morphogenesis. Cell 1996; 84:345-57.

10. Hartsock A, Nelson WJ. Adherens and tight junctions: structure, function and connections to the actin cytoskeleton. Biochimica et biophysica acta 2008; 1778:660-9.

11. Critchley DR. Focal adhesions - the cytoskeletal connection. Current opinion in cell biology 2000; 12:133-9.

12. Ridley AJ, Schwartz MA, Burridge K, Firtel RA, Ginsberg MH, Borisy G, Parsons JT, Horwitz AR. Cell migration: integrating signals from front to back. Science (New York, NY 2003; 302:1704-9.

13. Palecek SP, Loftus JC, Ginsberg MH, Lauffenburger DA, Horwitz AF. Integrin-ligand binding properties govern cell migration speed through cell-substratum adhesiveness. Nature 1997; 385:537-40.

14. Steinberg MS. On Mechanism of Tissue Reconstruction by Dissociated Cells .3. Free Energy Relations and Reorganization of Fused, Heteronomic Tissue Fragments. P Natl Acad Sci USA 1962; 48:1769-&.

15. Steinberg MS. Differential adhesion in morphogenesis: a modern view. Current opinion in genetics & development 2007; 17:281-6.

16. Steinberg MS, Foty RA. Intercellular adhesions as determinants of tissue assembly and malignant invasion. Journal of cellular physiology 1997; 173:135-9.

17. Lin MY, Lindsay HM, Weitz DA, Ball RC, Klein R, Meakin P. Universality in Colloid Aggregation. Nature 1989; 339:360-2.

18. Seinfeld J, Pandis S. *Atmospheric Chemistry and Physics: From Air Pollution to limate Change* (Wiley, Hoboken, 2006).

Chapter II. SHORT-LIVED CELL-CELL INTERACTIONS FOSTER TRANSPORT-LIMITED CELL AGGREGATION: BIPHASIC DEPENDENCE OF AGGREGATION DYNAMICS ON SUBSTRATUM ADHESIVITY

1. Abstract

Multicellular aggregation is fundamental to development and tissue repair.[1-3] The classical equilibrium model for multicellular aggregation is based on differential cell adhesivity to its neighbors versus the underlying substratum.[4-6] In many biological contexts, however, dynamics is critical. Here, we demonstrate that multicellular aggregation dynamics involves both local adhesive interactions and transport by cell migration. Quantitative measurements by time-lapse video microscopy reveal that the lifetime of cell-cell interactions is shorter than the mean time between cell-cell collisions, suggesting aggregation may be transport-limited. Consistent with this hypothesis, the transient aggregate size exhibits a biphasic dependence on substratum adhesivity, matching independent measurements of the trend in cell migration speed. These results demonstrate that cell aggregation adheres to a transport-reaction model ascribed widely to physicochemical systems.[7, 8] Our findings have implications for the role of cell motility during developmental aggregation processes and provide design principles for tuning aggregation dynamics in applications such as tissue engineering.

2. Main Text

Multicellular aggregation is fundamental to embryonic development and tissue repair,[1-3] and the loss of aggregate integrity is associated with pathologies such as metastasis.[9] The classical paradigm is that the equilibrium state of aggregation is determined by minimizing the adhesive free energy of the system.[4-6] This model predicts that if the cumulative strength of cell-cell adhesion (as quantified by the number and affinity of receptor-ligand bonds) exceeds the strength of cell-substratum adhesion, cells will organize into aggregates. Conversely, if the strength of cell-substratum adhesion exceeds the strength of cell-cell adhesion, cells will adopt a dispersed phenotype. This monotonic relationship between aggregation and substratum adhesivity has been demonstrated experimentally.[10] When cells of equal cohesivity are employed, those seeded onto weakly adhesive substrata aggregate while those seeded onto highly adhesive substrata dissociate.

In many biological contexts, however, the dynamics of aggregation is likely to be critical. The development of tissues and organs proceeds through multiple stages, and each step, such as multicellular aggregation, must be accomplished within a defined time window. When considering dynamics, it is well-established in physicochemical systems ranging from colloids[7] to atmospheric chemistry[8] that aggregation must be viewed as a two-step process (Figure II-1). The individual particles must first "find" each other (a transport step) and then form stable contacts (a reaction step). Aggregation dynamics is dictated by the slower of the two steps. It remains to be elucidated, however, whether cellular aggregation dynamics follows a similar principle.
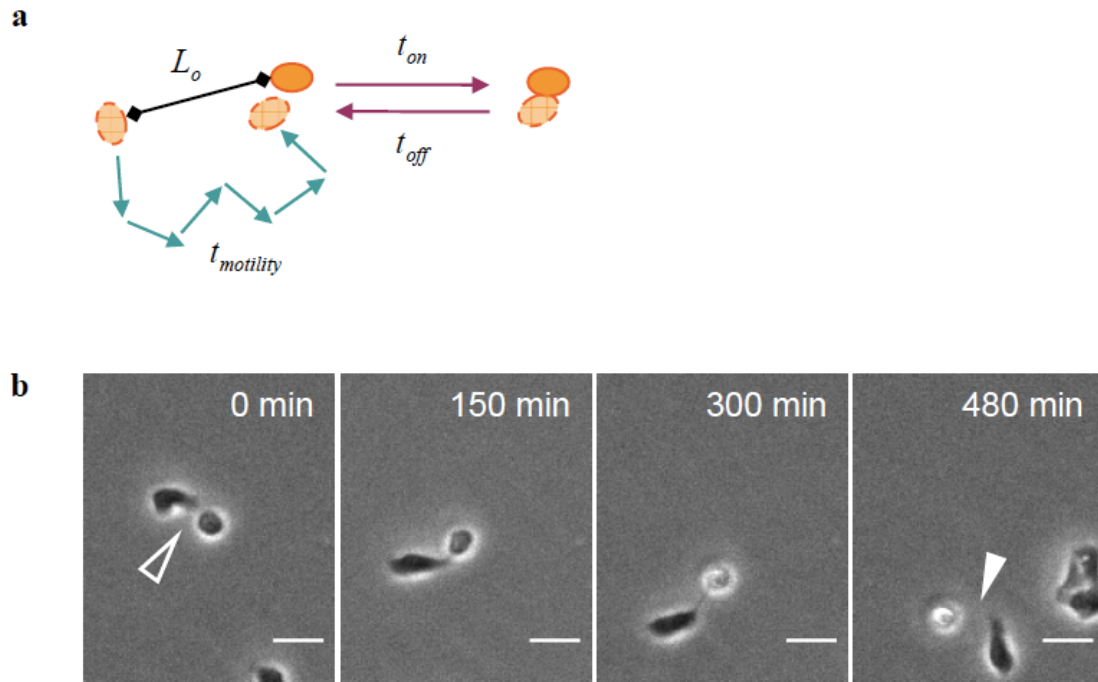
Figure II-1. Two-step model for multicellular aggregation dynamics.

(a) To form aggregates, distant cells must first move close together (a transport step) and then undertake reversible cell-cell interactions (a reaction step). Transport occurs by cell migration, and the mean time to collide ($t_{motility}$) depends on the mean initial spacing between cells (L_o) and the speed and persistence of cell movement. Meanwhile, the local cell-cell interaction involves adhesion (t_{on}) and detachment (t_{off}). (b) Timelapse images of migrating MDCK cells show the initiation of cell-cell contact (open arrowhead) and the subsequent detachment (closed arrowhead). Because t_{on} and t_{off} cannot be distinguished experimentally, timelapse images were used to quantify the total duration of cell-cell interactions ($t_{adhesion}$) as a lumped measure of t_{on} and t_{off}. Scale bar, 25 μm.

It is currently difficult to evaluate whether transport by cell migration or local cell-cell "reactivity" is the rate-limiting step in multicellular aggregation. In contrast to the large body of quantitative studies of cell migration[11], to our knowledge, there is currently no evaluation of the timescale on which migrating cells "react" to form intercellular contacts. Although cell-cell contact dynamics has been studied for cells brought together with micropipettes[12], interactions between migrating cells are likely to

be significantly different. Migrating cells interact with each other while concomitantly adhering to an underlying substratum. Furthermore, these cell-cell and cell-substratum adhesions involve common molecular components and physical machinery, such as actin and cell-generated contractile forces, respectively.[13, 14]

To quantify the dynamics of cell-cell interactions, we identified cell-cell collisions in time-lapse videos and recorded the duration of intercellular contact. These measurements were performed using substrata coated with different amounts of the adhesion ligand laminin (Ln) in order to better understand how varying substratum adhesivity affects the lifetime of cell-cell interactions. We observe that the mean lifetime of cell-cell interactions ($t_{adhesion}$) exhibits a monotonic dependence on substratum adhesivity (Figure II-2). Increasing adhesion ligand density reduces the lifetime of cell-cell interactions: $t_{adhesion}$ is nearly 600 min on substrata of low adhesivity and is reduced to approximately 200 min on substrata of high adhesivity. To confirm that our measurements are capturing specific cell-cell interactions, we treated cells with an antibody (DECMA) that blocks E-cadherin, a cell surface receptor that mediates intercellular adhesion. Treatment with DECMA reduces $t_{adhesion}$ compared to treatment with a non-specific IgG control, confirming that E-cadherin is involved in mediating these cell-cell interactions (Figure II-4, Supplemental Data).
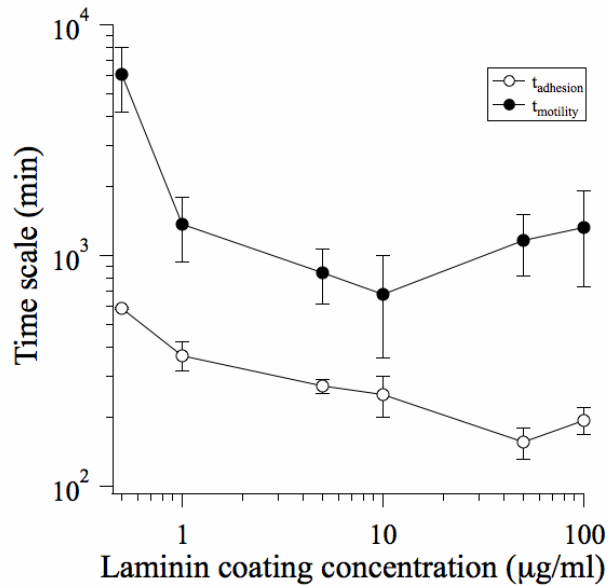
Figure II-2. The dependence of timescales of local cell-cell reactivity (tadhesion) and transport (tmotility) on substratum adhesivity.

The duration of cell-cell interactions ($t_{adhesion}$) and the mean time for nearest neighbors to collide ($t_{motility}$) were quantified for substrata prepared with different coating concentrations of Ln. Error bars, SEM (n = 2-3).

To assess how the measured lifetime of cell-cell interactions compares with the timescale of transport, we next examined cell migration on Ln-coated substrata. Cell migration in an isotropic environment exhibits an unbiased persistent random walk characterized by a diffusivity or motility coefficient (μ) that is related to the speed (S) and directional persistence (P) of cell movement.[15, 16] Migrating cells were tracked using time-lapse video microscopy, and cell speed was determined by fitting mean squared displacements to a persistent random walk model. Cell speed exhibits the expected biphasic dependence on substratum adhesivity.[11] In our system, the peak cell speed was 0.77 ± 0.09 μm/min on substrata coated with 10 μg/mL Ln (Figure II-5, Supplemental Data). The measured values of S and P (29.1 ± 6.4 min) are consistent with published values for epithelial cell lines.[17-19]

Using these values for S and P, we calculated the mean time required for a cell to collide with its nearest neighbor ($t_{motility} = L_o^2/\mu$) where $L_o \sim 108$ μm is the mean intercellular spacing based on the initial cell density of 8.5×10^3 cells/cm^2 and the motility coefficient μ is equal to S^2P. This time scale for transport exhibits a biphasic dependence on substratum adhesivity; therefore cell-cell collisions are infrequent on substrata of low and high adhesivity ($t_{motility} = 6.1 \pm 1.8 \times 10^3$ and $1.3 \pm 0.6 \times 10^3$ min, respectively) and occur with greatest frequency on substrata of moderate adhesivity ($t_{motility} = 6.8 \pm 3.2 \times 10^2$ min) (Figure II-2).

Comparing the measured time scales of transport and local reactivity reveals that $t_{motility}$ is greater than $t_{adhesion}$ across the complete range of Ln coating concentrations. Therefore, if multicellular systems follow the general two-step principle of aggregation dynamics, we would expect aggregation dynamics to exhibit a biphasic dependence on substratum adhesivity. Testing this hypothesis, however, is not straightforward. Varying substratum adhesivity will affect the number of seeded cells that attach to the substratum, thereby introducing unwanted differences in initial intercellular spacing. In addition, adequate time must be allowed for cells to attach to the substratum – a particularly important concern for substrata of low adhesivity. Furthermore, any non-adherent cells must be removed to ensure that the observed multicellular aggregation is the result of collisions between adherent, migrating cells and not between drifting cells in suspension. Guided by these and other considerations, we developed a rigorous protocol for studying the effect of substratum adhesivity on multicellular aggregation dynamics (Supplemental

Methods).   Our method yields highly uniform initial conditions: for all Ln coating concentrations, the initial density of substratum-attached cells was $8.5 \pm 0.2 \times 10^3$ #/cm^2 (Table II-1, Supplemental Data).

To quantify aggregate sizes, two-channel fluorescence images were acquired of multicellular aggregates stained with a nuclear and cell membrane marker.   The mean number of cells per aggregate was determined using previously described automated image processing techniques.[20]   We first performed a time course study to identify an appropriate time-point at which to examine the dynamics of our system.   Mean aggregate size was found to increase monotonically with time until reaching a plateau after 20 h of incubation (Figure II-6, Supplemental Data).   Therefore, we selected 15 h as an appropriate incubation time for capturing aggregation dynamics.

The mean aggregate size at 15 h exhibits a biphasic dependence on substratum adhesivity (Figure II-3).   Moreover, the maximum aggregate size occurs at the Ln coating concentration of 10 μg/ml, matching the conditions at which cell speed is maximum. These findings are consistent with a two-step physiochemical model for multicellular aggregation dynamics.   Furthermore, these data demonstrate that the time scale of local reactivity is sufficiently fast (200-600 min) to render aggregation dynamics transport-limited.   The consequence is that aggregation dynamics follows a non-monotonic dependence on substratum adhesivity, qualitatively contrary to the equilibrium perspective of the differential adhesion paradigm.
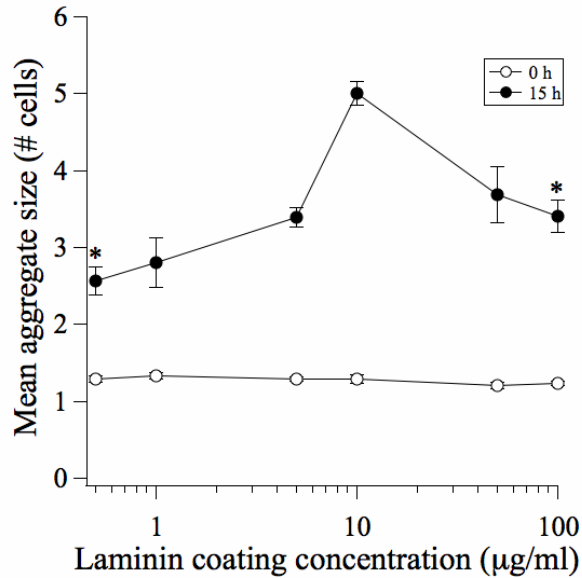
Figure II-3. Biphasic dependence of aggregate size on substratum adhesivity: evidence for motility-limited aggregation dynamics.

The mean aggregate size (# cells per aggregate) was quantified at initial time (0 h) and 15 h after the attachment of MDCK cells to Ln-coated substrata. Error bars, SEM (n = 3-4). *, $p < 0.05$ in comparing to the 10 µg/mL condition.

Our findings establish a key role for cell motility in multicellular aggregation. Evidence is also mounting for the role of cell motility in mediating another multicellular process: cell sorting of heterogeneous cell populations. Though proposed years ago as a potential mediator of cell sorting, differential motility has only recently been discussed as a driving mechanism for this phenomenon.[21, 22] A recent mathematical model of *Dictyostelium* slug formation, for example, demonstrates that motility differences among cell types are sufficient to create the defined spatial pattern of cells observed in migrating slugs.[23] In addition, cellular rearrangements within epithelial tissues have been attributed to differential motility: cells expressing high levels of the enzyme MMP14, which preferentially localize to the tip of epithelial tubes, were found to be faster and more directionally persistent than their low-expressing counterparts.[19] These studies of cell

sorting together with our results pertaining to cellular aggregation demonstrate the emerging importance of cell motility in the dynamics of multicellular re-arrangements.

In addition to natural developmental processes, our findings have direct implications for tissue engineering. Although engineering biomaterials with reduced adhesivity may enhance aggregation at equilibrium[24], we demonstrate that a qualitatively distinct strategy is needed to ensure optimal kinetics of aggregation. When dynamics is the chief concern, we propose that the design strategy must account for whether transport or local cell-cell reactivity is rate-limiting. Where transport is rate-limiting, a biomaterial with intermediate adhesivity will provide maximal aggregation dynamics. In conclusion, our results provide a dynamical physical perspective on engineering microenvironments to promote multicellular aggregation, an important precursor to more mature multicellular structures and tissues.

3. Acknowledgements

4. Materials and Methods

4.1. Substratum preparation

Tissue culture-treated polystyrene dishes (Corning) were incubated overnight at 4°C with laminin (Sigma) diluted in PBS. Prior to use, dishes were blocked with 1 mg/mL heat-inactivated (55 C for 1 hour) BSA (Sigma) in PBS at 37°C for 1 h.

4.2. Cell culture

MDCK cells were cultured in Dulbecco's modified Eagle's medium (DMEM, Invitrogen) supplemented with 10% (v/v) fetal bovine serum (Invitrogen) and 1% (v/v) penicillin/streptomycin (Invitrogen). For collision, motility and aggregation assays, confluent MDCK monolayers were suspended by treatment with 0.25% trypsin/53 mM EDTA (Invitrogen) for 5 minutes at 37 C and plated at the desired cell density in serum-free medium (SFM: DMEM supplemented with 1% (v/v) penicillin/streptomycin and 1 mg/mL BSA (Sigma)) supplemented with 20 ng/mL epidermal growth factor (EGF) (Peprotech). After allowing cells to adhere to the substratum for 1 – 3 hours, non-adherent cells were washed and the remaining adherent cells were incubated in fresh SFM supplemented with 20 ng/mL EGF.

4.3. Quantification of cell-cell adhesion dynamics

Samples were imaged via time-lapse microscopy using a Zeiss Axiovert 200M microscope equipped with a digital CCD camera and an environmental chamber that

maintains temperature, humidity and CO_2 levels. 5x phase contrast images were collected every 5 minutes for 24 hours. Cell-cell interactions that were initiated in the first 12 hours of observation were tracked, and the duration of cell-cell contact was recorded. Interacting cell pairs observed to collide with an additional cell or group of cells were excluded from the analysis.

4.4. Quantification of migration speeds

Migration tracks of individual cells were imaged by time-lapse microscopy. 10x phase contrast images were collected every 15 minutes for 15 hours. Nuclei of isolated cells were marked using ImageJ software (National Institutes of Health), and mean squared displacements were determined for each cell using overlapping intervals.[16] The mean squared displacements were averaged and fit to a persistent random walk model to calculate cell speed, S, and persistence time, P: $<d^2(t)> = 2S^2P[t-P(1-e^{-t/P})]$.[15, 16] Persistence was averaged across all laminin coating concentrations to determine a mean persistence time.

4.5. Quantification of aggregate size

Samples were fixed in formalin (Sigma), incubated overnight at 4 C in PBS + 100 mM glycine (Sigma), then permeabilized in PBS + 0.2% Triton-X for 10 minutes at 4 C. Cells were stained with DAPI and the membrane dye FM-464FX (Molecular Probes). Fluorescence images were captured at 10x magnification using a Zeiss Axiovert 200M microscope equipped with a digital CCD camera. 49 non-overlapping fields were imaged

per sample. Aggregate sizes were determined from these images using thresholding and edge detection algorithms as previously described.[20] The number of nuclei per field was also quantified in order to calculate the density of substratum-attached cells.

5. Supplemental Methods

In order to study how local cell-cell reactivity and transport by cell migration affect aggregation dynamics, it is essential to ensure that (1) isolated cells (not pre-formed aggregates) are seeded initially on the substrata, (2) any non-adherent cells are removed to prevent them from drifting and binding to adherent cells/aggregates, and (3) the initial density of isolated cells (and, therefore the initial mean intercellular spacing) is equal among all samples.

To address these considerations, MDCK cells were suspended using traditional cell dissociation techniques, and a desired concentration of single cells (N_c) was seeded onto Ln-coated substrata. After incubating cells for an appropriate duration (t_{inc}) to allow cell adhesion onto the substratum, non-adherent cells were removed by medium aspiration. The key issue, however, lies in determining the appropriate values for N_c and t_{inc} to ensure that the initial cell density on the substratum is equal for all Ln coating concentrations.

We reasoned that cell adhesion to a substratum is likely to proceed more quickly on substrata coated with higher Ln density than on those coated with low amounts of Ln based on reported measurements of cell spreading kinetics on protein-coated surfaces.[25] We quantified the dynamics of cell adhesion in our system (MDCK cells adhering to Ln-coated tissue culture plastic) (Figure II-7, Supplemental Data) and chose an incubation time that allows cell adhesion to reach its maximum saturation value for each Ln coating

concentration (Table II-2, Supplemental Data). This incubation time varied between 1-3 h and is much shorter than the time at which aggregation is quantified (15 h after t_{inc}).

In addition to the time of incubation, careful attention was given to the concentration of cells (N_c) seeded for each Ln coating concentration. We observed that the fraction of seeded cells that attach to the substratum at t_{inc} varied with Ln coating concentration (Figure II-8, Supplemental Data). Therefore, to ensure equivalent initial cell density among the different Ln-coated substrata, we seeded a greater concentration of cells (N_c) on substrata coated with lower amounts of Ln than on those coated with higher Ln density. Because the fraction of adherent cells was likely to also vary between trials, we took an additional precaution by performing each trial as follows: duplicate sets of cell suspensions containing three closely-spaced N_c were seeded for each Ln coating concentration (Table II-3, Supplemental Data). The first set of triplicates was used to determine the seeding concentration that yielded an initial cell density of approximately 8.5×10^3 #/cm^2. Once identified, the corresponding sample in the second set was used to determine aggregate size at 15 h. In this manner, we ensured that aggregation dynamics were quantified among samples that had an equivalent initial cell density (Table II-1, Supplemental Data).

6. Supplemental Data
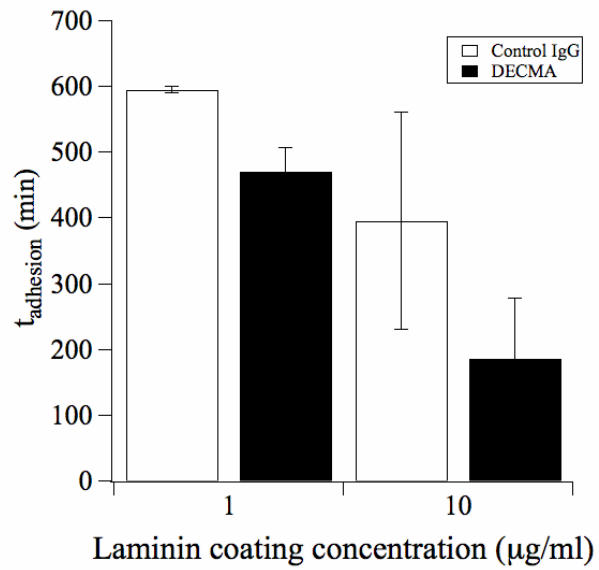
Figure II-4. Effect of antibody treatments on the lifetime of cell-cell interactions.

The lifetime of cell-cell adhesions ($t_{adhesion}$) was measured in the presence of an E-cadherin-specific or non-specific control IgG. Error bars, SEM (n = 2).
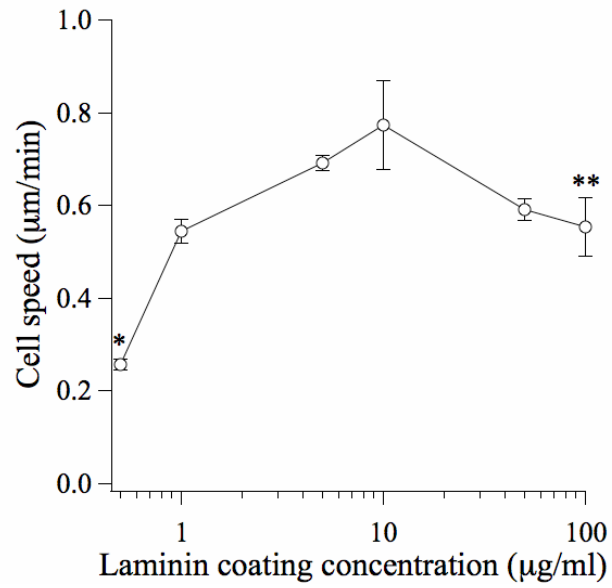
Figure II-5. Cell speed exhibits a biphasic dependence on surface adhesivity.

The migration tracks of individual MDCK cells were traced using timelapse microscopy. Mean squared displacements were calculated and fit to a persistent random walk model to determine cell speed.[15, 16] Error bars, SEM (n = 2). *, $p<0.05$ and **, $p<0.1$ in comparing to the 10 μg/mL condition.
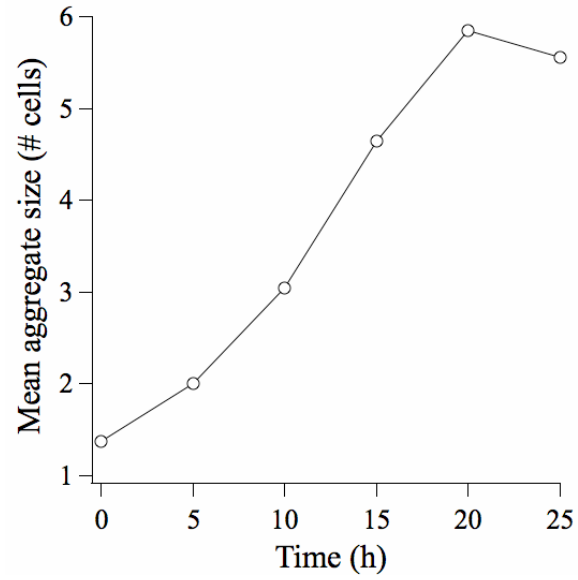
Figure II-6. Time-course of aggregate assembly.

The mean aggregate size (# of cells per aggregate) was quantified at initial time (0 h) and at multiple timepoints after the attachment of MDCK cells to the Ln-coated (10 µg/mL) substratum (n = 1).
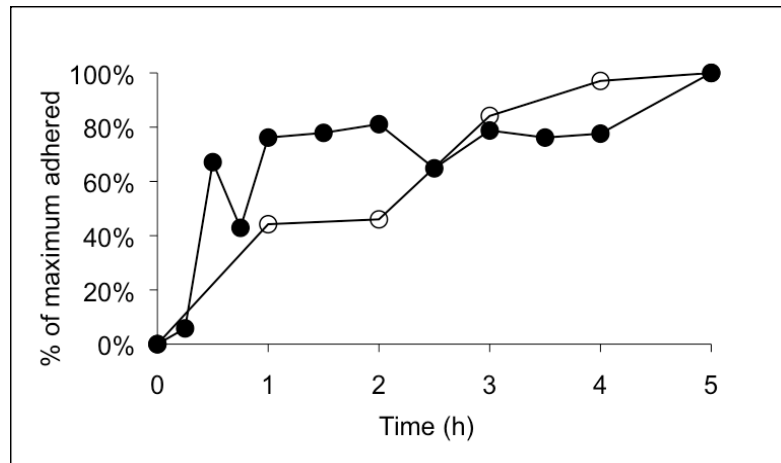
Figure II-7. Substratum adhesivity affects the rate of cell attachment to the substratum.

1.5×10^5 MDCK cells were seeded onto substrata coated with 0.5 µg/mL or 5 µg/mL Ln. After incubation for the indicated times, the non-adherent cells were washed, and the number of cells that remain attached was determined. The percent cells adhered relative to the maximum saturation value is shown (n = 1).
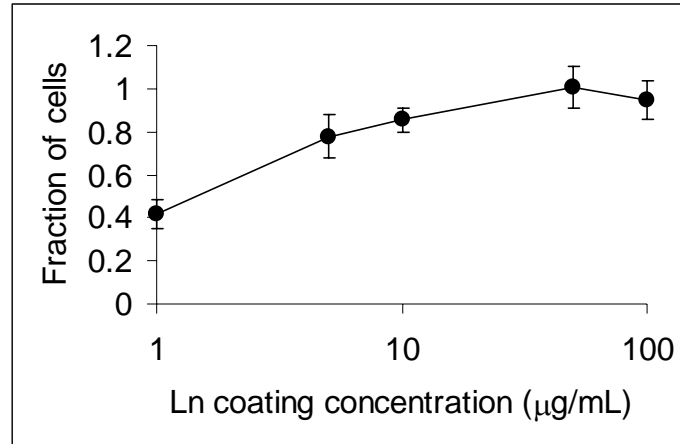
Figure II-8. Substratum adhesivity affects the fraction of seeded cells that attach.

1.0×10^5 MDCK cells were seeded onto Ln-coated substrata. The fraction of cells that attached to each substratum was quantified after incubation for t_{inc} (1 – 3 h) (n = 3-4).

Table II-1. Initial density of substratum-attached cells.

The number of substratum-attached cells per unit surface area was quantified at initial time (0 h) from fluorescence images of MDCK cells stained with DAPI. Error bars, SEM (n = 3-4).

Ln coating concentration (μg/mL)	0.5	1	5	10	50	100
Initial cell surface density x 10^{-3} (#/cm^2)	8.3 ± 0.78	8.2 ± 0.32	9.1 ± 0.50	8.9 ± 0.59	8.2 ± 0.59	8.2 ± 0.20

Table II-2. Incubation times for Ln-coated substrata.

Ln coating concentration (µg/mL)	0.5	1	5	10	50	100
t_{inc} (h)		3		2		1

Table II-3. Cell seeding concentrations for Ln-coated substrata.

	$N_c \times 10^{-4}$ (#/mL)					
Ln coating concentration (μg/mL)	3.75	5.0	6.75	7.5	10.0	12.5
0.5				X	X	X
1			X	X	X	
5		X	X	X		
10		X	X	X		
50	X	X	X			
100	X	X	X			

7. References

1. Gumbiner BM. Cell adhesion: the molecular basis of tissue architecture and morphogenesis. Cell 1996; 84:345-57.

2. Nakagawa S, Takeichi M. Neural crest cell-cell adhesion controlled by sequential and subpopulation-specific expression of novel cadherins. Development (Cambridge, England) 1995; 121:1321-32.

3. Oberlender SA, Tuan RS. Expression and functional involvement of N-cadherin in embryonic limb chondrogenesis. Development (Cambridge, England) 1994; 120:177-87.

4. Steinberg MS. On Mechanism of Tissue Reconstruction by Dissociated Cells .3. Free Energy Relations and Reorganization of Fused, Heteronomic Tissue Fragments. Proceedings of the National Academy of Sciences of the United States of America 1962; 48:1769-&.

5. Steinberg MS. Differential adhesion in morphogenesis: a modern view. Current opinion in genetics & development 2007; 17:281-6.

6. Steinberg MS, Foty RA. Intercellular adhesions as determinants of tissue assembly and malignant invasion. Journal of cellular physiology 1997; 173:135-9.

7. Lin MY, Lindsay HM, Weitz DA, Ball RC, Klein R, Meakin P. Universality in Colloid Aggregation. Nature 1989; 339:360-2.

8. Seinfeld J, Pandis S. *Atmospheric Chemistry and Physics: From Air Pollution to Climate Change* (Wiley, Hoboken, 2006).

9. Hanahan D, Weinberg RA. The hallmarks of cancer. Cell 2000; 100:57-70.

10. Ryan PL, Foty RA, Kohn J, Steinberg MS. Tissue spreading on implantable substrates is a competitive outcome of cell-cell vs. cell-substratum adhesivity. Proceedings of the National Academy of Sciences of the United States of America 2001; 98:4323-7.

11. Palecek SP, Loftus JC, Ginsberg MH, Lauffenburger DA, Horwitz AF. Integrin-ligand binding properties govern cell migration speed through cell-substratum adhesiveness. Nature 1997; 385:537-40.

12. Sung KL, Sung LA, Crimmins M, Burakoff SJ, Chien S. Determination of junction avidity of cytolytic T cell and target cell. Science 1986; 234:1405-8.

13. Hartsock A, Nelson WJ. Adherens and tight junctions: structure, function and connections to the actin cytoskeleton. Biochimica et biophysica acta 2008; 1778:660-9.

14. Ridley AJ, Schwartz MA, Burridge K, Firtel RA, Ginsberg MH, Borisy G, Parsons JT, Horwitz AR. Cell migration: integrating signals from front to back. Science 2003; 302:1704-9.

15. Dickinson RB, Tranquillo RT. Optimal Estimation of Cell-Movement Indexes from the Statistical-Analysis of Cell Tracking Data. Aiche J 1993; 39:1995-2010.

16. Walmod PS, Hartmann-Petersen R, Berezin A, Prag S, Kiselyov VV, Berezin V, Bock E. Evaluation of individual-cell motility. Methods in molecular biology (Clifton, NJ 2001; 161:59-83.

17. Li Y, Bhargava MM, Joseph A, Jin L, Rosen EM, Goldberg ID. Effect of hepatocyte growth factor/scatter factor and other growth factors on motility and

morphology of non-tumorigenic and tumor cells. In vitro cellular & developmental biology 1994; 30A:105-10.

18. Maheshwari G, Wiley HS, Lauffenburger DA. Autocrine epidermal growth factor signaling stimulates directionally persistent mammary epithelial cell migration. The Journal of cell biology 2001; 155:1123-8.

19. Mori H, Gjorevski N, Inman JL, Bissell MJ, Nelson CM. Self-organization of engineered epithelial tubules by differential cellular motility. Proceedings of the National Academy of Sciences of the United States of America 2009; 106:14890-5.

20. Pope MD, Graham NA, Huang BK, Asthagiri AR. Automated quantitative analysis of epithelial cell scatter. Cell adhesion & migration 2008; 2:110-6.

21. Stefanelli A ZA CV. Retinal reconstitution in vitro after disaggregation of embryonic chicken eyes. Acta Embryol Morphol Exper 1961; 4:47-55.

22. Townes PL, Holtfreter J. Directed Movements and Selective Adhesion of Embryonic Amphibian Cells. J Exp Zool 1955; 128:53-120.

23. Umeda T, Inouye K. Cell sorting by differential cell motility: a model for pattern formation in Dictyostelium. Journal of theoretical biology 2004; 226:215-24.

24. Powers MJ, Rodriguez RE, Griffith LG. Cell-substratum adhesion strength as a determinant of hepatocyte aggregate morphology. Biotechnology and bioengineering 1997; 53:415-26.

25. Dubin-Thaler BJ, Giannone G, Dobereiner HG, Sheetz MP. Nanometer analysis of cell spreading on matrix-coated surfaces reveals two distinct cell states and STEPs. Biophysical journal 2004; 86:1794-806.

Chapter III. AUTOMATED QUANTITATIVE ANALYSIS OF EPITHELIAL CELL SCATTER

1. Abstract

Epithelial cell scatter is a well-known *in vitro* model for the study of epithelial-mesenchymal transition (EMT). Scatter recapitulates many of the events that occur during EMT, including the dissociation of multicellular structures and increased cell motility. Because it has been implicated in tumor invasion and metastasis, much effort has been made to identify the molecular signals that regulate EMT. To better understand the quantitative contributions of these signals, we have developed metrics that quantitatively describe multiple aspects of cell scatter. One metric (cluster size) quantifies the disruption of intercellular adhesions while a second metric (nearest-neighbor distance) quantifies cell dispersion. We demonstrate that these metrics delineate the effects of individual cues and detect synergies between them. Specifically, we find epidermal growth factor (EGF), cholera toxin (CT) and insulin to synergistically reduce cluster sizes and increase nearest-neighbor distances. To facilitate the rapid measurement of our metrics from live-cell images, we have also developed automated techniques to identify cell nuclei and cell clusters in fluorescence images. Taken together, these studies provide broadly applicable quantitative image analysis techniques and insight into the control of epithelial cell scatter, both of which will contribute to the understanding of EMT and metastasis.

2. Introduction

Epithelial cells have an intrinsic ability to self-assemble into multicellular structures. For example, submandibular gland (SMG) epithelial cells isolated from embryonic mice retain the ability to self-organize into branched tissue aggregates in a manner analogous to that which occurs *in vivo*.[1] These epithelial tissues have a distinct, well-ordered structure. Namely, constituent cells tightly adjoin to their neighbors and form highly polarized multicellular sheets that provide physical barriers between external and internal environments. In addition, epithelial cells are motile, in that they can move away from their neighbors, but generally remain within the epithelial layer.[2]

Many epithelial tissues are dynamic structures that undergo constant regeneration. Disruptions in the self-assembly and maintenance of epithelial cell structures can have drastic pathological consequences such as cancer development.[3] These physical disruptions are driven by molecular perturbations that alter cell behavior. For example, oncogenes such as *c-met* break up cellular aggregates and promote cell dispersion.[4] At a single cell level, these molecular perturbations induce an epithelial-mesenchymal transition (EMT). During EMT, epithelial cells lose apical-basolateral polarity and transform into a more migratory phenotype, resembling fibroblasts. This allows cells to dissociate from the epithelial layer and disperse.[5]

Because of the clinical and physiological significance of EMT, much effort has been made to identify the molecular signals that control this process. An important tool for the *in vitro* study of EMT is the cell scatter assay, in which two-dimensional epithelial

aggregates dissociate in response to extracellular stimuli. While advances are being made in cataloguing the signaling pathways that control scatter, an emerging challenge is to understand the quantitative contributions of these signals and any coupling between them. For example, which stimuli are the most potent effectors? Which signals work synergistically? Which signals work antagonistically?

A challenge to answering these questions is that current studies of cell scatter are largely qualitative. Prevalent in the limited quantitative literature are studies that score cellular aggregates as "scattered" based on an observed morphological change – for example the appearance of space between cells, the disappearance of membrane-localized desmoplakin or a reduction in the number of cell-cell adhesions.[6-9] Such analyses permit comparison between experimental conditions but provide little insight into the cellular-level response.

In this work, we introduce quantitative metrics to systematically characterize multiple aspects of epithelial cell scatter. One metric is the aggregate size, which quantifies the degree to which cells have disrupted intercellular adhesions. Another metric is the distance between a cell and its nearest neighbor, which evaluates the extent to which cells disperse. Our data shows that these metrics delineate the effects of individual molecular signals and detect synergies between them. Specifically, we find epidermal growth factor (EGF) to be essential for scattering non-transformed human mammary epithelial cells (MCF-10A) and to synergize with both cholera toxin (CT) and insulin to reduce aggregate size and increase internuclear distances. To facilitate the

rapid measurement of our metrics from live-cell images, we have also developed automated techniques to identify cell nuclei and multicellular aggregates in fluorescence images. In summary, this work provides an experimental methodology and high throughput techniques that will prove useful for gleaning quantitative insights into EMT.

3. Results

3.1. EGF regulates MCF-10A scatter

When deprived of the soluble factors contained in growth medium (GM), MCF-10A cells aggregate into well-defined clusters (Figure III-1A). Upon re-addition of GM, cells scatter (Figure III-1B). GM has several components, among them EGF, which has been shown to induce scatter in multiple cell lines.[7, 8, 10, 11] When EGF is omitted from GM, cell scatter is noticeably reduced (Figure III-1C). However, EGF alone is unable to induce scatter (Figure III-1D). Therefore, EGF appears to be required for scatter but not sufficient to induce a response. We next performed a qualitative screen to identify additional components of GM that contribute to scatter. Among them were CT and insulin. CT appears to synergize with EGF to induce scatter (Figure III-1E), while the further addition of insulin makes little noticeable enhancement (Figure III-1F) even after comparing across 16 different fields (Supplemental Data). Thus, based on this qualitative analysis, we conclude that (1) although EGF is essential for cell scatter, it alone does not induce cell scatter, and (2) CT, but not insulin, significantly synergizes with EGF to induce cell scatter. To test these assessments more rigorously, we sought to quantify the extent of cell scatter induced by these different treatments.
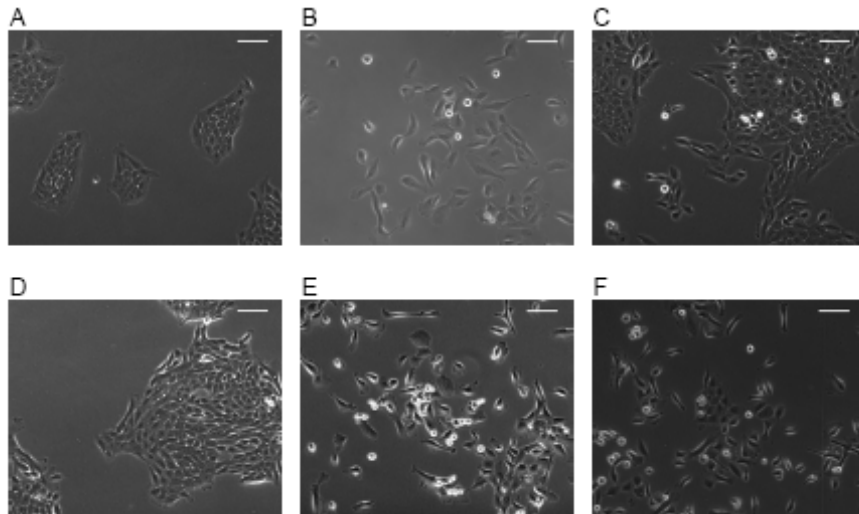
Figure III-1. EGF is a key regulator of epithelial cell scatter.

(A) MCF-10A cells were maintained in SFM for 24 hours to induce the formation of multicellular aggregates. To induce scatter, aggregates were then treated for 24 hours with multiple soluble factors. GM (B), EGF + CT (E) and EGF + CT + insulin (F) induce cell scatter, while EGF (D) and GM containing all factors except for EGF (C) do not. EGF, CT and insulin were used at concentrations identical to those of GM: 20 ng/ml, 100 ng/ml, and 10 μg/ml respectively. Scale bars are 100 μm.

3.2. Quantitative metrics of cell scatter

We propose two metrics to quantify the extent of cell scatter. The first metric is the number of cells in a cluster, i.e. the cluster size. A cell cluster is defined as a group of cells in which every member is in physical contact with at least one other member. This metric quantifies the degree to which cells have disrupted intercellular adhesions. Therefore, the mean cluster size is expected to decrease as cells scatter. This metric would not, however, effectively gauge the degree to which cells have dispersed. Thus, a loosely disaggregated cluster would score equivalently to a completely scattered population. To address this issue, we propose a second metric, the nearest-neighbor distance, to evaluate cell dispersion. The nearest-neighbor distance measures the distance

between a cell and its nearest neighbor. We expect the mean nearest-neighbor distance to increase as cells scatter. This metric of cell scatter would have a lower limit (the diameter of a single cell) and an upper limit that depends on the surface density of cells.

3.3. The distribution of cluster sizes is differentially altered by EGF-containing media

After serum-starvation, the distribution of cluster sizes is bimodal, with one peak centered at small sizes (2-5 cells per cluster) and a second peak centered at moderate sizes (20-30 cells per cluster) (Figure III-2A). Upon treatment with EGF for 24 hours, the fraction of isolated cells (i.e. 1 cell per cluster) remains unchanged. This confirms that EGF is not sufficient to disrupt multicellular aggregates (Figure III-1D). However, unexpectedly, treatment with EGF dramatically reduces the fraction of cells in small- and moderate-sized clusters (2-70 cells per cluster), leading to the emergence of a new population of large aggregates (100+ cells per cluster) (Figure III-2B).

This observation from our quantitative measurements led us to probe several mechanisms that may underlie these changes. One possibility is that proliferation within small- and moderate-sized aggregates causes an increase in cluster size. Because MCF-10A proliferation occurs on a timescale of 18 hours post-treatment with EGF, we would expect proliferation effects in our experiments to be minimal. Indeed, we find that these large aggregates form even in the presence of aphidicolin, an inhibitor of proliferation (data not shown). A second possibility is that small- and moderate-sized clusters aggregate to form large ones. To test this possibility, we collected time-lapse videos of

serum-starved cells treated with EGF. These videos clearly show the amalgamation of small/moderate-sized aggregates into large aggregates (Figure III-2C). It therefore appears that although EGF is required for scatter, treatment with this factor alone promotes the formation of new cell-cell adhesions and the amalgamation of pre-existing aggregates.

Treatment with CT in conjunction with EGF increases the fraction of cells that are isolated or in small clusters after 24 hours compared to treatment with EGF alone. This result is consistent with the apparent cell scatter induced by co-treatment with EGF and CT (Figure III-1E). Furthermore, inclusion of CT reduces the formation of new large clusters. CT therefore synergizes with EGF in both disrupting cell-cell adhesions and reducing the formation of new adhesions.

The further addition of insulin results in nearly complete dissociation of moderate-sized aggregates (15-100 cells per cluster), and predominantly small clusters and isolated cells remain after 24 hours. Thus, insulin makes a striking contribution to the disruption of cell clusters that was not evident from our qualitative analysis (Figure III-1F). Our quantitative measurements reveal that insulin-mediated signals are essential for maximum scatter.

Notably, GM, which in addition to EGF, CT and insulin contains serum and hydrocortisone, is a less potent promoter of scatter than EGF + CT + insulin. This

suggests that additional components contained within GM may counteract insulin-mediated effects and reduce scatter.

Figure III-2. Distribution of cluster sizes for scattering cells.

MCF-10A cells were maintained in SFM for 24 hours to induce the formation of multicellular aggregates. (A, B) Aggregates were treated with the indicated factor(s) for 24 hours to induce scatter. 15 – 30 epifluorescence images were acquired per condition per experiment and cluster size was determined for all clusters completely contained within an image (150 – 250 clusters per condition per experiment). EGF, EGF + CT and GM induce the formation of large aggregates (100+ cells per cluster) while SFM and EGF + CT + insulin do not. Note that since the fraction of cells in aggregates of 100+ cells is equal to zero for the SFM and EGF + CT + insulin conditions, they are not included in Figure III-2B. Data are means ± standard error; n=3. Asterisk denotes p <

0.05 (Student's t test) in comparing the fraction of cells that are isolated after treatment with EGF + CT to the fraction of cells that are isolated after culture in SFM and comparing the fraction of cells that are isolated after treatment with GM to the fraction of cells that are isolated after culture in SFM. (C) Aggregates were treated with EGF and imaged via time-lapse microscopy for 24 hours. Arrowheads indicate locations where new adhesions are formed. Scale bars are 100 μm.

3.4. The distribution of nearest-neighbor distances is differentially altered by EGF-containing media

After serum-starvation, nearly every cell is a member of an aggregate and therefore in contact with its nearest neighbor. Upon stimulation with EGF-containing media, the fraction of cells in contact with their nearest neighbor (i.e. a nearest-neighbor distance of ≤ 1 cell diameter) decreases (Figure III-3). EGF alone produces little change in the distribution of nearest-neighbor distances. However, the additions of CT and insulin produce stepwise increases in the fraction of cells that have distanced themselves from their neighbors by multiple cell diameters. GM induces the greatest response, scattering a small population of cells by greater than 2 cell diameters.
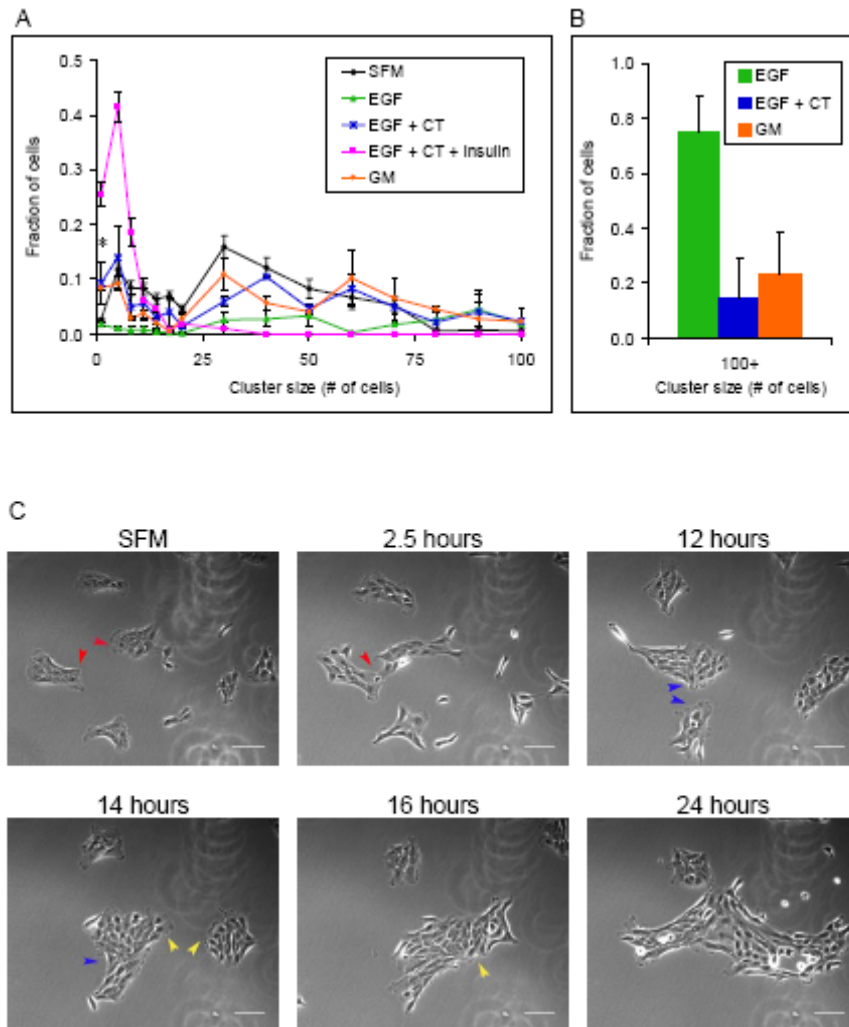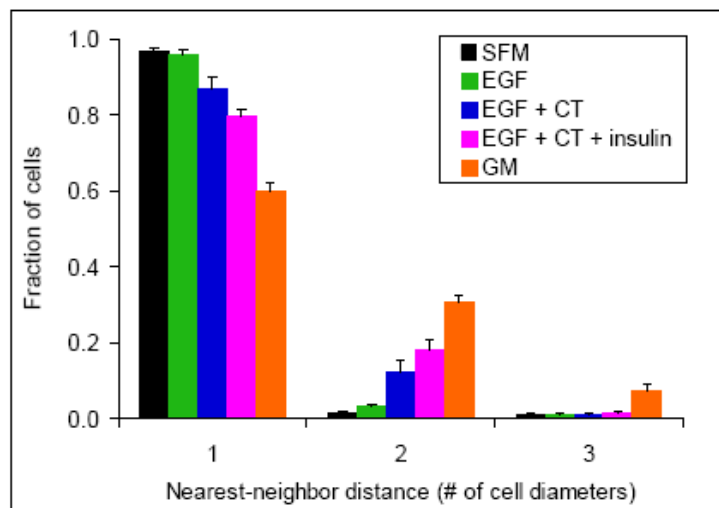
Figure III-3. Distribution of nearest-neighbor distances for scattering cells.

MCF-10A cells were maintained in SFM for 24 hours to induce the formation of multicellular aggregates. Aggregates were then treated with the indicated factor(s) and imaged via time-lapse microscopy for 24 hours. Nearest-neighbor distances were determined for all cells within the first (SFM) and last frames. A cell diameter was taken to be the greatest nearest-neighbor distance measured for contacting serum-starved cells (42 μm), and all nearest-neighbor distances were expressed as multiples of this distance. Data are means ± standard error; n=2.

To determine if the measured nearest-neighbor distances approach those expected at maximal scatter, we calculated a theoretical maximum internuclear distance that corresponds to the case where all cells are equally spaced from one another. This distance was calculated as follows: the surface area contained within an image was divided by the number of cells within the image to determine an area per cell. Assuming each cell to be a circle of the resulting area with a nucleus at its center, the maximum internuclear distance was calculated to be 76.9 ± 4.8 μm or ~1.8 cell diameters. Therefore, the distances presented in Figure III-3 approach the values expected at the time of maximal scatter.

3.5. Automated image processing

From the data presented above, it is clear that our metrics provide useful quantitative insight into the regulation of epithelial cell scatter and exhibit promise for use in future studies. The manual measurement of these metrics, however, is time-consuming. We have therefore developed a simple, high throughout method for identifying cell nuclei and multicellular aggregates in fluorescence images.

MCF-10A cells expressing nuclear-localized GFP and membrane-localized mCherry were imaged using epifluorescence and a digital CCD camera (Figure III-4A,A'). GFP-channel intensity images were segmented using the MATLAB function edge. Edge creates a binary image with 1's where the function finds edges and 0's elsewhere. Next, the function imfill was used to fill holes (areas of black pixels surrounded by white pixels) in the segmented images (Figure III-4B). This algorithm correctly reconstructs isolated nuclei, but fails to resolve contacting nuclei into distinct structures. In fact, contact between nuclei is occasionally created by under-segmentation. To address this issue, the watershed algorithm was applied to the image and successfully divides overlapping nuclei into distinct objects.[12]
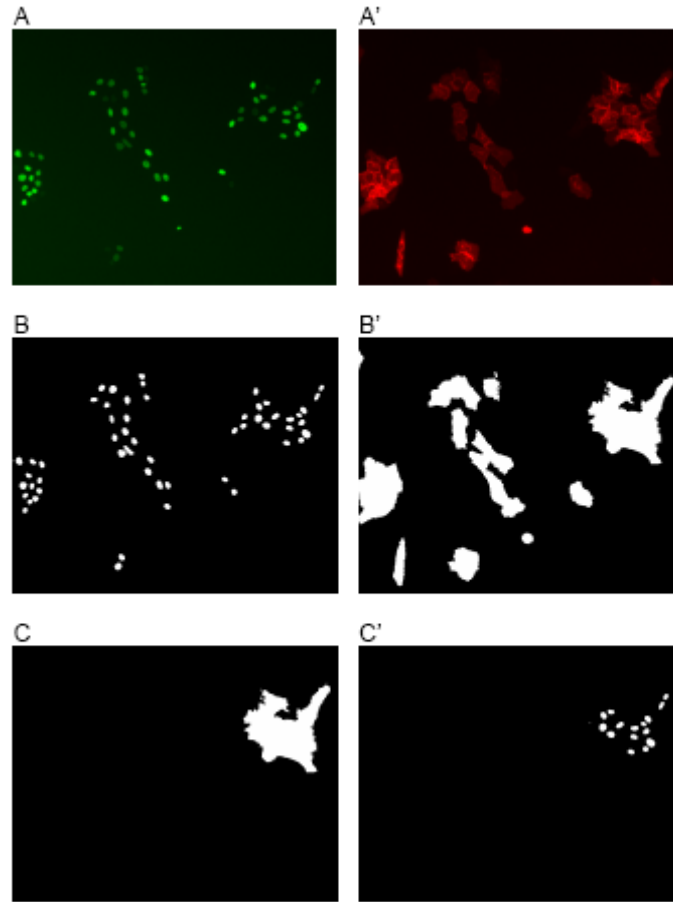
Figure III-4. Automated image processing using MATLAB.

(A, A') Nuclear- and membrane-localized fluorescent proteins, H2B-GFP and mCherry respectively, were co-expressed in MCF-10A cells. (B, B') Epifluorescence images of scattering cells were segmented using thresholding and edge detection algorithms in MATLAB. (C) Masks were created such that each mask contained a single cluster. (C') Masks were then applied to the corresponding H2B-GFP image and nuclei that co-localized with the mask were identified. These nuclei were counted to determine the cluster size.

To identify cell clusters, a global threshold was applied to red-channel intensity images using the MATLAB function graythresh. Graythresh computes a global threshold for each image using Otsu's algorithm.[13] This method correctly identifies all cell clusters, but also introduces additional small objects into the image. To eliminate these non-cellular components, a size threshold was applied to the image using the function

bwareaopen. Objects smaller than the area of a single cell (~400 μm^2) were eliminated from the image, resulting in a binary image containing distinct cell clusters (Figure III-4B').

Cluster size and nearest-neighbor distance metrics were easily and quickly extracted from the processed images. To determine cluster sizes, clusters in membrane-mCherry frames were first indexed using the function bwlabel. Bwlabel creates a matrix in which pixels labeled 0 make up the background, pixels labeled 1 make up one object, pixels labeled 2 make up a second object, and so on. From each indexed image, a series of masks was created such that each mask contained a single cluster (Figure III-4C). Masks were then applied to the corresponding H2B-GFP image and the nuclei overlapping with each were indexed and counted using bwlabel (Figure III-4C'). To determine nearest-neighbor distances, nuclear centroids were determined from the segmented H2B-GFP frames using the function regionprops. Internuclear distances were calculated and the minimum distance measured for each cell was recorded.

We next performed a trial experiment to determine the precision with which these automated techniques evaluate our metrics. Scattering MCF-10A cells co-expressing H2B-GFP and membrane-mCherry were imaged via phase contrast and epifluorescence. Cluster sizes and nearest-neighbor distances were determined (1) manually from phase contrast images and (2) from fluorescence images of the same fields using the described automated method. For both the SFM and GM conditions, results obtained via automated image processing were similar to those obtained manually (Figure III-5).
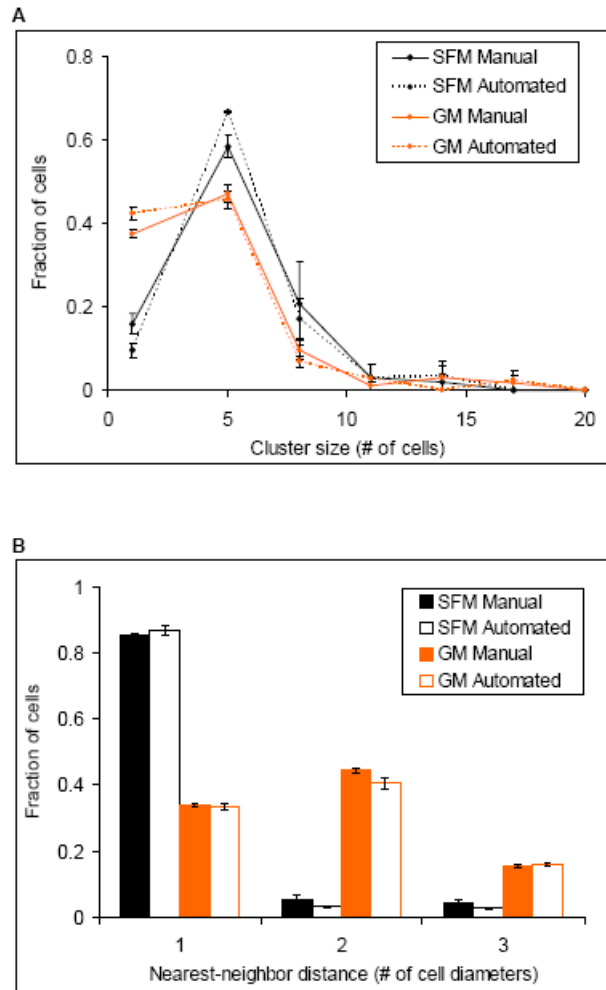
Figure III-5. Comparison of manual and automated techniques.

MCF-10A cells co-expressing H2B-GFP and membrane-mCherry were maintained in SFM for 24 hours to induce the formation of multicellular aggregates. Aggregates were then treated with GM for 24 hours to induce scatter. For each field, both phase contrast and epifluorescence images were collected.   Cluster sizes (A) and nearest-neighbor distances (B) were determined manually from phase contrast images and from epifluorescence images using the described automated techniques. Both cluster size and nearest-neighbor distance distributions are similar for the manual and automated techniques.

We note that for each application (i.e. cell line and stimulation conditions), one must also test whether the H2B-GFP and membrane-mCherry constructs perturb cell behavior. This is best accomplished by comparing cluster sizes and nearest-neighbor distances determined manually for uninfected cells to those determined manually for cells expressing the fluorescent constructs.

4. Discussion

Epithelial organization is regulated by a complex signaling network. Many scatter-promoting factors have been identified, among them EGF, hepatocyte growth factor (HGF), fibroblast growth factor (FGF) and transforming growth factor β (TGF-β). These extracellular cues trigger various intracellular signals – Src, Rac, PI3K and Erk, for example – that drive scatter.[3, 14, 15] A key limiting factor in our understanding of this phenomenon is that the phenotypic changes associated with scatter are characterized largely in qualitative terms. Such assessment is inadequate for several reasons. First, qualitative characterizations do not provide insight into how important a particular factor might be. Is the degree of scatter induced by EGF the same as that induced by HGF? Is there quantitative synergy when both signals are received? Second, cell scatter is a complex phenomenon involving several events. These events include de-compaction of the aggregate, cell-cell dissociation and cell migration. However, because cell scatter is currently evaluated in a lumped fashion, the precise facet(s) of cell scatter a given signal affects remain unclear.

This work introduces quantitative metrics to describe multiple aspects of epithelial cell scatter. We demonstrate that these metrics gauge the potencies with which specific signals induce scatter and the synergies among them. Our measurements show that although EGF alone is unable to induce cell scatter, it synergizes with CT to reduce aggregate sizes and increase nearest-neighbor distances. Furthermore, our quantitative metrics extracted information regarding the role of insulin that would be missed from a qualitative analysis. Inspecting images of cells treated with EGF, CT and insulin suggested that insulin provided no major enhancement to the scatter induced by EGF and CT. However, quantitative measurements of cluster sizes and nearest-neighbor distances revealed that insulin provides a striking improvement in cell scatter, essentially ablating all clusters. This type of quantitative analysis will prove useful for categorizing scatter-promoting factors according to their ability to alter epithelial structures and for grouping synergistic cues. Moreover, identifying potent scatter-inducing cues may provide more pivotal targets for anti-cancer therapeutics.

This quantitative approach also provides new insights into the role of EGF in multicellular epithelial organization. Our measurements revealed that treatment with EGF alone induced the formation of large aggregates through the amalgamation of small/moderate-sized aggregates. Thus, although EGF is essential for inducing cell scatter in the presence of co-factors, our data suggest that EGF alone promotes cell-cell adhesion and the emergence of large clusters.

The metrics proposed in this study quantify distinct aspects of scatter, and therefore, may not always be correlated to each other. For example, GM treatment does not score as the most efficient at breaking clusters apart (Figure III-2), but still mediates the largest increase to nearest-neighbor distance (Figure III-3). This counterintuitive observation is due to a phenomenon called de-compaction, where cells in a cluster relax cell-cell adhesions and enhance cell spreading against the substratum. In this manner, GM-treated cells distance themselves from their neighbors without breaking cell-cell contacts. Thus, the proposed metrics gauge distinct aspects of multicellular organization and analyzing how both metrics respond to molecular perturbations can provide mechanistic insights.

Because the metrics capture distinct facets of cell scatter, they will prove useful in exploring synergisms between signals. Some cues, for instance, will have a profound effect on breaking cell-cell contacts but little effect on the nearest-neighbor distance. Other cues will have exactly the opposite effect. Combined exposure to such complementary cues may have a synergistic effect on cell scatter that is significantly greater than their individual contributions. Identifying such synergistic cues may reveal "multi-hit" pathways that contribute to cancer development and thereby guide therapeutic strategies.

In this work, we also present a simple, versatile and high-throughput method for measuring morphological changes to epithelial structures from live-cell images. These techniques may be a valuable tool not only for in-depth study of cell scatter, but also for

clinical applications. First, quantitative metrics combined with automated image analysis may facilitate *in vitro* high-throughput screening of anti-cancer therapeutics. Furthermore, since inspection of tumor morphology is widely used to categorize disease and decide on a treatment option, the techniques described here may facilitate advancements in cancer diagnostics.[3, 5] Overall, we believe our methods can provide necessary quantitative insight into the regulation of epithelial structures, which will lead to advancements in our understanding of scatter, EMT and metastasis.

5. Materials and Methods

5.1. Cell culture

MCF-10A cells were cultured in Dulbecco's modified Eagle's medium/Ham's F-12 containing HEPES and L-glutamine (Invitrogen) supplemented with 5% (v/v) horse serum (Invitrogen), 20 ng/ml EGF (Peprotech), 0.5 µg/ml hydrocortisone (Sigma), 0.1 µg/ml cholera toxin (Sigma), 10 µg/ml insulin (Sigma), and 1% penicillin/streptomycin (Invitrogen). For serum starvation, cells were washed twice with PBS and then cultured in Dulbecco's modified Eagle's medium/Ham's F-12 supplemented with 1% (v/v) penicillin/streptomycin and 0.1% bovine serum albumin (Sigma) for 24 h.

5.2. Plasmid Constructs

H2B-GFP and membrane-mCherry were gifts from S. Fraser (California Institute of Technology). The membrane-mCherry construct consists of monomeric mCherry fused to the first 20 amino acids of zebrafish Gap43.[16] Palmitoylation at cysteine residues within the Gap43 sequence directs the mCherry protein to the membrane.[17, 18] VSV-G and gag-pol vectors were gifts from D. Schaffer (University of California, Berkeley).

5.3. Retroviral Infection

H2B-GFP and membrane-mCherry genes were subcloned into retroviral vectors (pLHCX and pLPCX respectively) and expressed in epithelial cell lines via retroviral

infection. Retrovirus was produced by triple transfection of 293T cells with 5 μg each of VSV-G, gag-pol and the retroviral vector using LipofectAMINE (Invitrogen). For infection, cells were incubated with retrovirus-containing medium and 8 μg/ml polybrene for 24 h. Puromycin (2 μg/mL) and hygromycin (100 μg/mL) were used for selection.

5.4. Cell scatter assay

MCF-10A cells were seeded in GM at a density of 8×10^4 per 35 mm culture dish and, 18-24 hours later, serum starved for 24 hours to induce aggregate formation. Cell aggregates were then stimulated with the indicated factor(s) and imaged. MCF-10A cells co-expressing membrane-mCherry and H2B-GFP were seeded at 2×10^4 per 35 mm dish.

5.5. Live cell microcopy

Images were captured at 10x magnification using a Zeiss Axiovert 200M microscope equipped with a digital CCD camera. Time-lapse microscopy experiments were performed using an environmental chamber that maintains temperature, humidity and CO_2 levels.

6. Supplemental Data
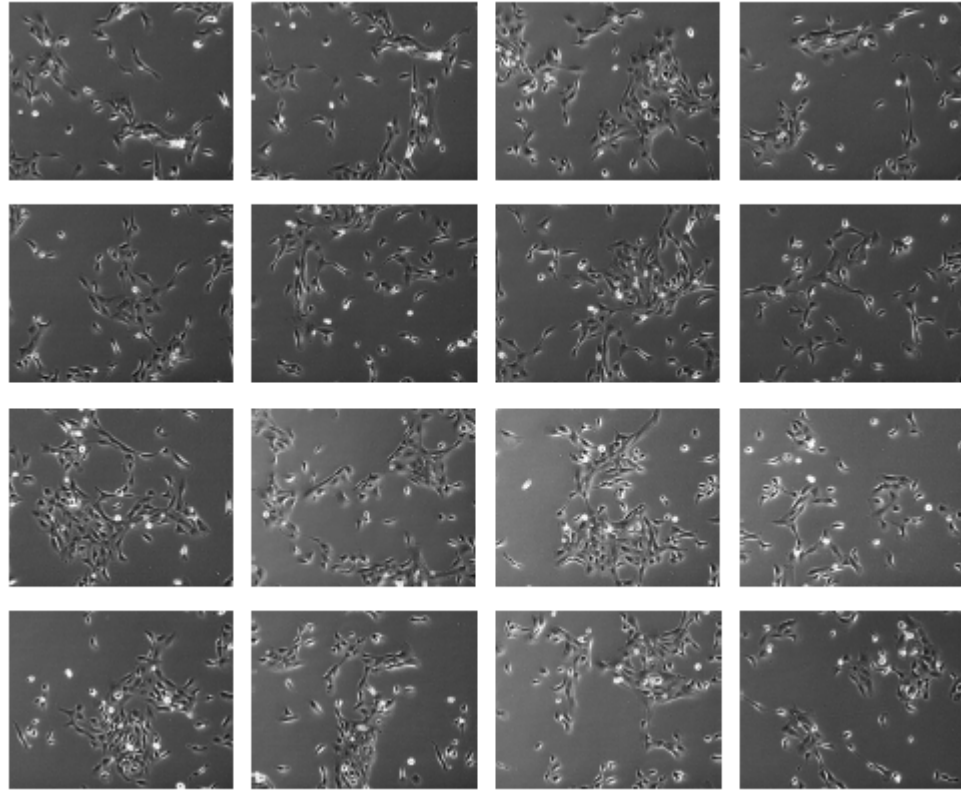
Figure III-6. Phase contrast images of MCF-10A cell aggregates treated with EGF + CT.

MCF-10A cells were maintained in SFM for 24 hours to induce the formation of multicellular aggregates. Aggregates were then treated with EGF + CT for 24 hours to induce scatter and imaged via phase contrast microscopy.
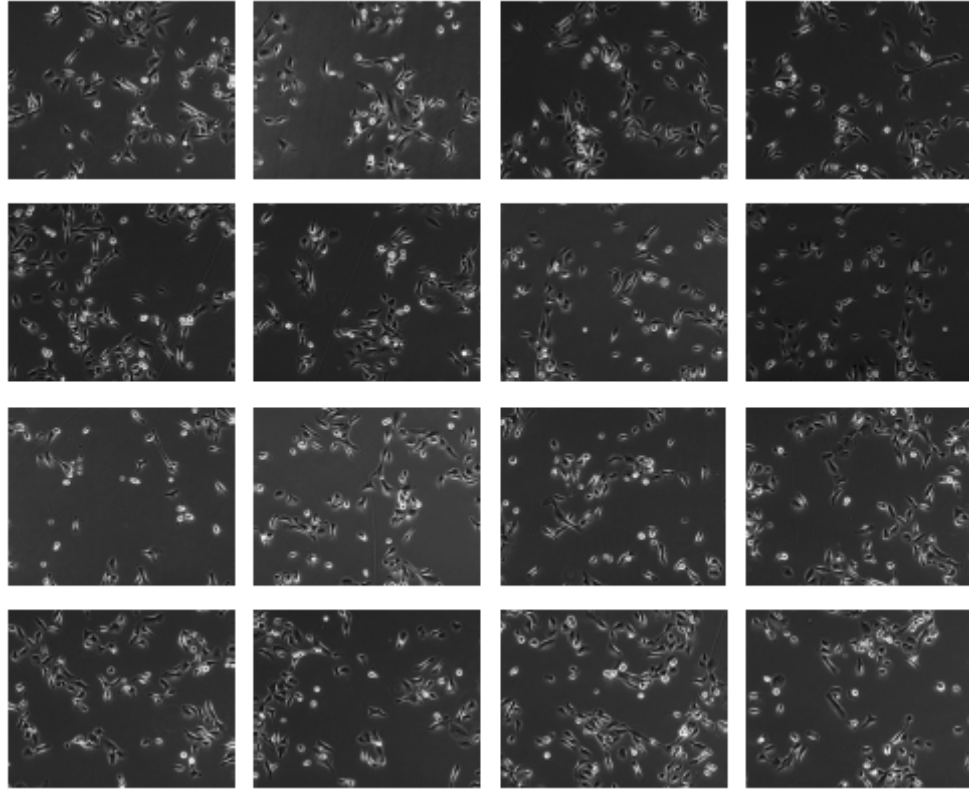
Figure III-7. Phase contrast images of MCF-10A cell aggregates treated with EGF + CT + insulin.

MCF-10A cells were maintained in SFM for 24 hours to induce the formation of multicellular aggregates. Aggregates were then treated with EGF + CT + insulin for 24 hours to induce scatter and imaged via phase contrast microscopy.

7. References

1. Wei C, Larsen M, Hoffman MP, Yamada KM. Self-organization and branching morphogenesis of primary salivary epithelial cells. Tissue engineering 2007; 13:721-35.

2. Schock F, Perrimon N. Molecular mechanisms of epithelial morphogenesis. Annual review of cell and developmental biology 2002; 18:463-93.

3. Thiery JP. Epithelial-mesenchymal transitions in tumour progression. Nature reviews 2002; 2:442-54.

4. Ma PC, Maulik G, Christensen J, Salgia R. c-Met: structure, functions and potential for therapeutic inhibition. Cancer metastasis reviews 2003; 22:309-25.

5. Vincent-Salomon A, Thiery JP. Host microenvironment in breast cancer development: epithelial-mesenchymal transition in breast cancer development. Breast Cancer Res 2003; 5:101-6.

6. Jourquin J, Yang N, Kam Y, Guess C, Quaranta V. Dispersal of epithelial cancer cell colonies by lysophosphatidic acid (LPA). Journal of cellular physiology 2006; 206:337-46.

7. Boyer B, Roche S, Denoyelle M, Thiery JP. Src and Ras are involved in separate pathways in epithelial cell scattering. The EMBO journal 1997; 16:5904-13.

8. Edme N, Downward J, Thiery JP, Boyer B. Ras induces NBT-II epithelial cell scattering through the coordinate activities of Rac and MAPK pathways. Journal of cell science 2002; 115:2591-601.

9.   de Rooij J, Kerstens A, Danuser G, Schwartz MA, Waterman-Storer CM. Integrin-dependent actomyosin contraction regulates epithelial cell scattering. The Journal of cell biology 2005; 171:153-64.

10.   Lu Z, Ghosh S, Wang Z, Hunter T. Downregulation of caveolin-1 function by EGF leads to the loss of E-cadherin, increased transcriptional activity of beta-catenin, and enhanced tumor cell invasion. Cancer cell 2003; 4:499-515.

11.   Matthay MA, Thiery JP, Lafont F, Stampfer F, Boyer B. Transient effect of epidermal growth factor on the motility of an immortalized mammary epithelial cell line. Journal of cell science 1993; 106 (Pt 3):869-78.

12.   Gonzales R, Woods R, Eddins S. Image Segmentation. In: O'Brian V, ed. Digital Image Processing using MATLAB. Upper Saddle River, NJ: Pearson Prentice Hall, 2004.

13.   McAndrew A. Image Segmentation. In: Mendelsohn M, ed. Introduction to Digital Image Processing with MATLAB. Boston, MA: Thomson Course Technology, 2004.

14.   Christofori G. New signals from the invasive front. Nature 2006; 441:444-50.

15.   Thiery JP, Sleeman JP. Complex networks orchestrate epithelial-mesenchymal transitions. Nat Rev Mol Cell Biol 2006; 7:131-42.

16.   Shaner NC, Campbell RE, Steinbach PA, Giepmans BN, Palmer AE, Tsien RY. Improved monomeric red, orange and yellow fluorescent proteins derived from Discosoma sp. red fluorescent protein. Nature biotechnology 2004; 22:1567-72.

17.   Skene JH, Virag I. Posttranslational membrane attachment and dynamic fatty acylation of a neuronal growth cone protein, GAP-43. The Journal of cell biology 1989; 108:613-24.

18.   Zuber MX, Goodman DW, Karns LR, Fishman MC. The neuronal growth-associated protein GAP-43 induces filopodia in non-neuronal cells. Science (New York, NY 1989; 244:1193-5.

Chapter IV. A MICROTITER ASSAY FOR QUANTIFYING PROTEIN-PROTEIN INTERACTIONS ASSOCIATED WITH CELL-CELL ADHESION

1. Abstract

Cell-cell adhesions are a hallmark of epithelial tissues, and the disruption of these contacts plays a critical role in both the early and late stages of oncogenesis. The interaction between the transmembrane protein E-cadherin and the intracellular protein β-catenin plays a crucial role in the formation and maintenance of epithelial cell-cell contacts, and is known to be down-regulated in many cancers. We have developed a protein complex enzyme-linked immunosorbent assay (ELISA) that can quantify the amount of β-catenin bound to E-cadherin in unpurified whole cell lysates with a Z' factor of 0.74. The quantitative nature of the E-cadherin:β-catenin ELISA represents a dramatic improvement over the low-throughput assays currently used to characterize endogenous E-cadherin:β-catenin complexes. In addition, the protein-complex ELISA format is compatible with standard sandwich ELISAs for parallel measurements of total levels of endogenous E-cadherin and β-catenin. In two case studies closely related to cancer cell biology, we utilize the protein complex ELISA and traditional sandwich ELISAs to provide a detailed, quantitative picture of the molecular changes occurring within adherens junctions *in vivo*. Because the E-cadherin:β-catenin protein complex plays a crucial role in oncogenesis, this protein complex ELISA may prove to be a valuable quantitative prognostic marker of tumor progression.

2. Introduction

Cell-cell adhesions are an integral aspect of epithelial tissues. These adhesions provide a physical barrier between two compartments, permitting the epithelial cell layer to serve as a selective transporter. Moreover, the attenuation of cell-cell adhesion plays a critical role in both early and late stages of oncogenesis.[1] At early steps, reduced intercellular adhesion may attenuate contact-inhibition of proliferation, permitting unchecked cell division and tumor formation; at later stages, reduced cell-cell adhesion is often associated with invasion, metastasis, and poor patient prognosis.[2]

In epithelial tissues, adherens junctions play a central role in the establishment and maintenance of cell-cell adhesions.[3] These junctions are composed of the cadherin and catenin families of proteins, which link sites of cell-cell contact to the actin cytoskeleton. Cadherins are transmembrane proteins that bind homotypically to cadherins on neighboring cells; meanwhile, the intracellular tail of cadherins binds β-catenin, which then recruits α-catenin and links to the actin cytoskeleton. In epithelial tissues, E- (epithelial) cadherin is the predominant member of the cadherin family expressed, and the loss of E-cadherin via genetic and epigenetic mechanisms is common in tumor progression.[4]

Given their integral role in forming and maintaining cell-cell adhesion, the interaction of E-cadherin and β-catenin has been widely studied. The most common method for assaying the expression and subcellular localization of endogenous E-cadherin and β-catenin in pathological contexts is histochemistry.[5, 6] While informative,

these methods are low-throughput and offer only qualitative information. Other more quantitative approaches have been developed to examine the molecular mechanisms governing E-cadherin:β-catenin association, including bead-based co-immunoprecipitation techniques (co-IP),[7-9] semi-quantitative immunofluorescence,[10] recombinant protein pull-down assays,[11, 12] and chip-based biosensors.[13] Co-IP assays, in particular, have been widely used to measure the association of endogenous E-cadherin and β-catenin; however, this technique involves cumbersome and repetitive centrifugation and wash steps, as well as low-throughput handling of multiple test tubes. Furthermore, the proteins isolated by co-IP are typically analyzed by Western blotting, which offers a limited linear range of detection. In contrast, other techniques using recombinant proteins provide quantitative measures of E-cadherin:β-catenin interactions over a wide linear range;[12, 13] however, these *in vitro* binding assays may not reflect *in vivo* biology.

We have developed a protein complex enzyme-linked immunosorbent assay (ELISA) that addresses many of the limitations in current methods for quantifying the amount of endogenous E-cadherin:β-catenin complexes. The microtiter format is also highly compatible with the standard sandwich ELISA for parallel measurements of total protein levels. In two case studies closely related to cancer cell biology, we demonstrate that the protein complex ELISA, in conjunction with parallel measurements of total protein, offers a detailed, quantitative picture of the molecular changes occurring within adherens junctions *in vivo*.

3.   Results and Discussion

3.1. Development and validation of a quantitative microtiter ELISA for E-cadherin:β-catenin protein complexes

Changes in E-cadherin:β-catenin interactions modulate cell-cell interactions and contribute to cell invasiveness and epithelial-mesenchymal transition.[1] To better quantify the level of E-cadherin:β-catenin association, we sought to develop a microtiter immunoassay built on the format of the traditional sandwich ELISA. In contrast to the sandwich ELISA, which measures the levels of a single protein, the protein complex ELISA quantifies the level of an endogenous protein complex, as has been previously described for several other protein complexes.[14-16] The assay utilizes an antibody to capture an antigen from unpurified whole cell lysate, similar to a sandwich ELISA; however, rather than employ a detection antibody against the captured antigen, as in a sandwich ELISA, the protein complex ELISA utilizes a detection antibody targeting a purported binding partner of the captured antigen. For example, to measure the E-cadherin:β-catenin protein complex, one might use an anti-E-cadherin antibody for the initial capture step, followed by an anti-β-catenin antibody for detection of β-catenin associated with the captured E-cadherin. Thus, although both free and β-catenin-bound E-cadherin would be captured in the initial step, the protein complex ELISA is designed to selectively detect β-catenin in complex with E-cadherin. The amount of detection antibody can then be measured using an alkaline phosphatase-conjugated secondary antibody and the colorimetric substrate p-nitrophenyl phosphate (PNPP), where the rate

of change in optical density at 405 nm provides a quantitative measure of detection antibody present.

The protein complex ELISA hinges on the possibility that capturing an antigen from crude cell lysates will co-precipitate associated proteins. This co-precipitation is exploited in IP-based detection of protein-protein complexes, a technique that involves the low-throughput, cumbersome use of test tubes in repeated centrifugation and wash steps. To verify that co-precipitation would occur in a microtiter format, we used a monoclonal anti-E-cadherin antibody to capture E-cadherin from whole cell lysate and subsequently treated the wells with SDS sample buffer to extract all proteins. For this initial test, we used lysates from an immortalized mammary epithelial cell line (MCF-10A) that forms adherens junctions rich in E-cadherin:β-catenin complexes.

Analyzing protein extracts from microtiter wells by SDS-PAGE and Western blot demonstrated that the anti-E-cadherin monoclonal antibody efficiently captured E-cadherin from whole cell lysates (Figure IV-1A). Importantly, β-catenin co-precipitated with E-cadherin; in fact, the amount of β-catenin increased with the amount of whole cell lysate used in the assay. Furthermore, the 'reverse' co-capture also worked in the microtiter format (Figure IV-1B). Using a monoclonal anti-β-catenin antibody as the capture antibody allowed efficient capture of β-catenin and associated E-cadherin. Again, the amount of captured β-catenin and co-captured E-cadherin increased with the amount of whole cell lysate used in the assay, suggesting that co-capture may have a broad dynamic range.
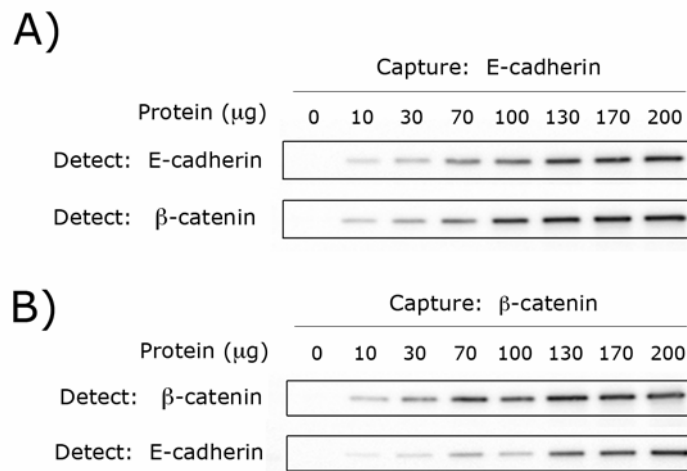
Figure IV-1. Antigen capture and protein:protein co-capture.

Mouse monoclonal antibodies against either (A) E-cadherin or (B) β-catenin were adsorbed to a microtiter plate, and varying amounts of whole cell lysates from MCF-10A cells were incubated in the wells. Protein fractions isolated by the capture antibodies were collected and analyzed by Western blot for the presence of E-cadherin or β-catenin.

While the co-captured protein is detectable by Western blot after stripping the wells, it is not clear whether the amount of co-captured protein is sufficient to detect using the microtiter immunoassay protocol. To address this question, we applied the protein complex ELISA to detect the amount of β-catenin that is bound to E-cadherin. We used a monoclonal anti-E-cadherin antibody to capture E-cadherin from cell lysate and then detected co-captured β-catenin using a polyclonal anti-β-catenin antibody. The protein complex ELISA exhibits a linear response over the entire range of whole cell lysate used in this study (0 - 200 μg) (Figure IV-2A). Furthermore, the amount of β-catenin co-captured with E-cadherin was detectable in as little as 10 μg of whole cell lysate, and the signal/noise ratio was approximately 8 (Table IV-1). Indicative of the

protein complex ELISA's robustness, the statistical parameter used for evaluation of high-throughput screens (Z') for this E-cadherin:β-catenin ELISA was 0.74.
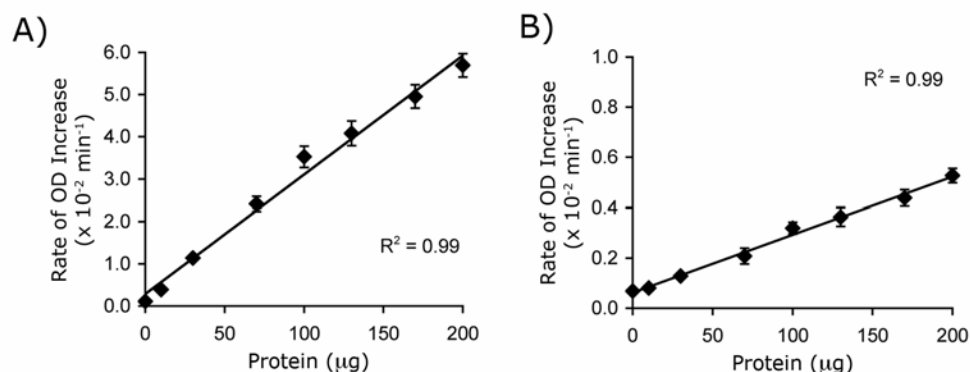
Figure IV-2. Detection of E-cadherin:β-catenin protein complexes by protein complex ELISA.

Whole cell lysate from MCF-10A cells was analyzed by protein complex ELISA for E-cadherin:β-catenin complexes by either (A) E-cadherin capture or (B) β-catenin capture. The rate of change in the optical density over time was plotted versus total cell lysate, and a linear regression was performed. Error bars represent the sample standard error (n = 3).

We also tested the reverse protein complex ELISA by capturing β-catenin with the mouse monoclonal antibody and then detecting E-cadherin with a polyclonal anti-E-cadherin antibody. The β-catenin:E-cadherin ELISA also demonstrated a broad linear dynamic range over 0 - 200 μg of whole cell lysate (Figure IV-2B). However, the β-catenin:E-cadherin format was slightly less sensitive than the E-cadherin:β-catenin ELISA, as the signal/noise ratio of this assay was only 6.2 (Table IV-1). However, this assay still demonstrates good suitability to screening assays, with a Z' factor of 0.59.

The relatively poorer performance of the β-catenin:E-cadherin ELISA is consistent with the full profile of *in vivo* protein:protein interactions in which β-catenin and E-cadherin participate. Whereas the β-catenin-binding domain of E-cadherin also recruits plakoglobin, a close homolog of β-catenin,[3] the Armadillo repeat domains of β-catenin bind numerous proteins including α-catenin, Tcf/Lef and components of the Axin-APC degradation machinery.[17] Thus, in principle, for a fixed E-cadherin:β-catenin binding affinity in a particular cell lysate, captured E-cadherin should generate more co-captured β-catenin signal than the co-capture of E-cadherin by β-catenin. However, while this physiological explanation could explain the better performance of the E-cadherin:β-catenin ELISA, we cannot rule out assay-related issues, such as relatively poorer efficacy of the monoclonal capture antibody for β-catenin versus E-cadherin.

Table IV-1. Quantitative performance of protein complex and sandwich ELISAs

Assay type	Captured protein	Detected protein	Signal/Noise ratio [a]	Z′ factor [a]
Protein complex ELISAs	E-cadherin	β-catenin	7.7	0.74
	β-catenin	E-cadherin	6.2	0.59
Sandwich ELISAs	E-cadherin	E-cadherin	48	0.80
	β-catenin	β-catenin	3.6	0.19

[a] Calculated as described in Materials and Methods.

The results reported for the protein complex ELISAs were collected using optimal assay conditions; all other formats and conditions tested were found to be sub-optimal in terms of signal strength and signal/noise ratio. For example, we attempted to increase the amount of properly-oriented capture antibody coated on the well by first adsorbing

neutravidin, followed by incubation with a biotinylated secondary antibody that would bind the Fc domain of the capture antibody. Although this approach has been reported to increase antigen capture elsewhere,[18] the neutravidin/biotin approach reduced the signal/background ratio of our protein complex ELISA by approximately 5-fold compared to direct adsorption of the capture antibody (data not shown).

The reduced sensitivity resulted from a non-specific interaction between neutravidin and the alkaline phosphatase-conjugated secondary antibody used in the detection phase of the assay. In other stages of assay development, we observed that the monoclonal antibody outperformed the polyclonal antibody in the capture step. For example, in the case of the E-cadherin:β-catenin ELISA, using the mouse monoclonal antibody for antigen capture step yielded a ~6-fold higher signal/background ratio than when the rabbit polyclonal antibody was used for capture (data not shown). Additionally, we explored the effect of the incubation temperature on assay sensitivity, but protein complex ELISAs carried out at 4 ºC and 37 ºC showed no difference in assay sensitivity (data not shown). All results reported here are from assays conducted at 37 ºC.

To verify that the protein complex ELISA specifically measures the interaction of E-cadherin and β-catenin, we performed the E-cadherin:β-catenin ELISA but omitted portions of the capture antibody:protein complex:detection antibody bridge that presumably forms in the microtiter well. Omission of either the cell lysate, the anti-E-cadherin capture antibody, or the anti-β-catenin detection antibody completely ablated the assay signal (Figure IV-3), demonstrating that a measurable assay signal is produced

only when the complete antibody:protein:antibody sandwich is established. Given that these antibodies specifically recognize only one protein in Western blots (data not shown), combined with the fact that these antibodies can mediate capture of protein complexes in a microtiter well (Figure IV-1), this demonstrates that the protein complex ELISA is specifically measuring the interaction of E-cadherin and β-catenin.
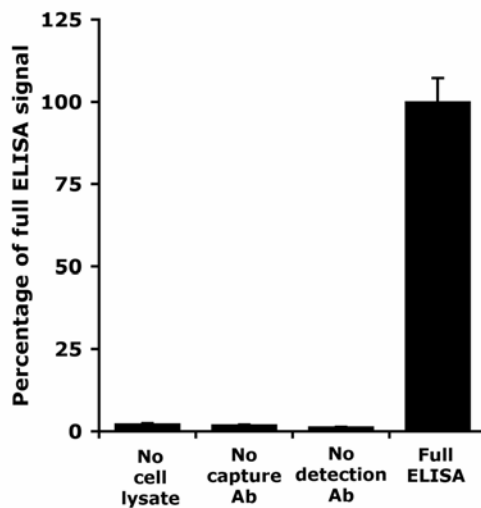
Figure IV-3. Specificity test for E-cadherin:β-catenin ELISA.

The E-cadherin:β-catenin ELISA was performed on 100 μg of MCF-10A whole cell lysate. At the appropriate step, either the whole cell lysate, the anti-E-cadherin capture antibody (Ab), or the anti-β-catenin detection antibody was omitted from the assay. Values are presented as the percentage of the rate of change in optical density over time relative to the control ELISA, where no reagents were omitted (Full ELISA). Error bars represent the sample standard error (n = 3).

3.2. Compatibility of the protein complex ELISA with standard sandwich ELISAs

Our results demonstrate that the protein complex ELISA offers a quantitative method for measuring the amount of endogenous E-cadherin:β-catenin complexes in crude cell lysates. A key consideration, however, is that any measured change in the

level of protein:protein complexes may be to due to a change in either protein:protein affinity or protein expression level. To discriminate between these possibilities, it is essential to measure the total amount of each protein in whole cell lysates. To address this issue, we exploited the flexibility of the protein complex ELISA to accommodate the traditional sandwich ELISA.

Having demonstrated that both E-cadherin and β-catenin are captured effectively in microtiter wells (Figure IV-1), we determined whether the amount of captured antigen may be detected using polyclonal anti-E-cadherin and anti-β-catenin antibodies in a sandwich ELISA format. Under the optimal detection conditions, E-cadherin was detected over a linear range spanning a wide range of whole cell lysate (0 - 130 μg) (Figure IV-4A). Notably, the linear range of the E-cadherin sandwich ELISA extended only to 130 μg, as opposed to the protein complex ELISAs, which demonstrated linearity to at least 200 μg of total cell protein. The linear dynamic range of the standard sandwich ELISA may saturate at a lower amount of total cell protein compared to the protein complex ELISA because not all E-cadherin molecules are bound to β-catenin and vice-versa. Nonetheless, the E-cadherin sandwich ELISA demonstrated an outstanding signal/noise ratio of 48, with a Z' factor of 0.80 (Table IV-1). Using the same conditions as in the E-cadherin sandwich ELISA, we tested the detection of β-catenin using monoclonal and polyclonal anti-β-catenin antibodies for capture and detection, respectively. As for E-cadherin, β-catenin detection was linear up to 130 μg of total cell protein (Figure IV-4B), with a signal/noise ratio of 3.6 (Table IV-1). The β-catenin ELISA, in contrast to the E-cadherin sandwhich ELISA, appears only marginally suitable

for screening assays, with a Z' factor of only 0.19. However, these results show that the protein complex ELISA is readily compatible with the sandwich ELISA for detecting total protein levels. This compatibility suggests that these assays may be operated on the same microtiter platform in parallel, reducing interplate variabilities and enhancing measurement throughput.
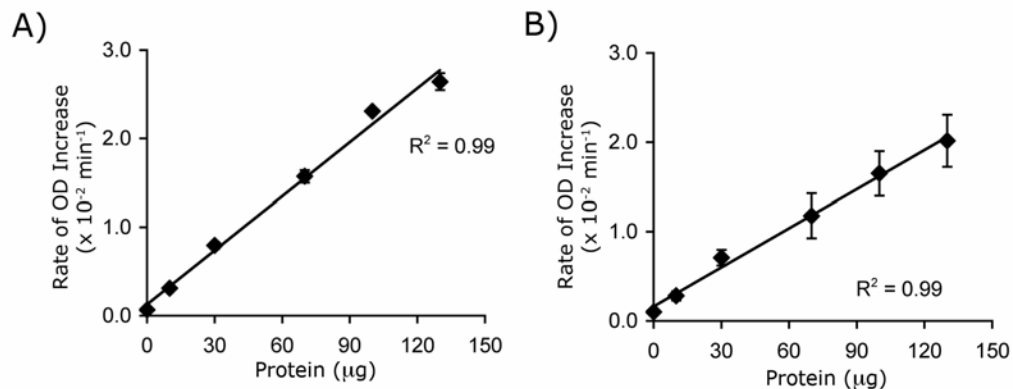
Figure IV-4. Detection of E-cadherin and β-catenin total protein levels by sandwich ELISA.

Whole cell lysate from MCF-10A cells was analyzed by sandwich ELISA for (A) total E-cadherin expression or (B) total β-catenin expression. The rate of change in optical density over time was plotted versus total cell lysate, and a linear regression was performed. Error bars represent the sample standard error (n = 3).

3.3. Quantitative comparison of E-cadherin:β-catenin interactions in transformed versus non-transformed cells

To test the applicability of the protein complex and the total protein ELISAs, we quantified the amount of E-cadherin:β-catenin complexes and the expression level of E-cadherin and β-catenin in a transformed and a non-transformed cell system. The non-transformed mammary epithelial cell line, MCF-10A, exhibits a normal epithelial

phenotype, including E-cadherin-mediated intercellular adhesion;[19] meanwhile, SW480 is a colon carcinoma cell line with a dysfunctional β-catenin degradation machinery that permits β-catenin to build up to high levels in the cytoplasm.[20]

To confirm that SW480 cells express greater amounts of β-catenin than MCF-10A cells, we used the β-catenin sandwich ELISA. The β-catenin sandwich ELISA yielded a linear response with respect to the amount of whole cell lysate load in the assay for both cell types (Supplementary Figure IV-1). We quantified the slope of the ELISA signal versus the amount of whole cell lysate as a metric of the amount of β-catenin. As shown in Figure IV-5A, the amount of β-catenin per μg of cell lysate was nearly 10-fold higher in SW480 cells than in MCF-10A cells, consistent with the known dysfunction of β-catenin degradation in SW480 cells.

We next examined how excessive stabilization of β-catenin might affect the level of E-cadherin:β-catenin complexes in SW480 cells relative to those found in the MCF-10A cell line. As shown in Figure IV-5B, the E-cadherin:β-catenin ELISA revealed that MCF-10A cells exhibit approximately 2-fold higher levels of E-cadherin:β-catenin complexes than SW480 cells. Thus, despite a 10-fold relative abundance in β-catenin expression, the amount of E-cadherin:β-catenin complexes is fewer in SW480 cells than in MCF-10A cells.
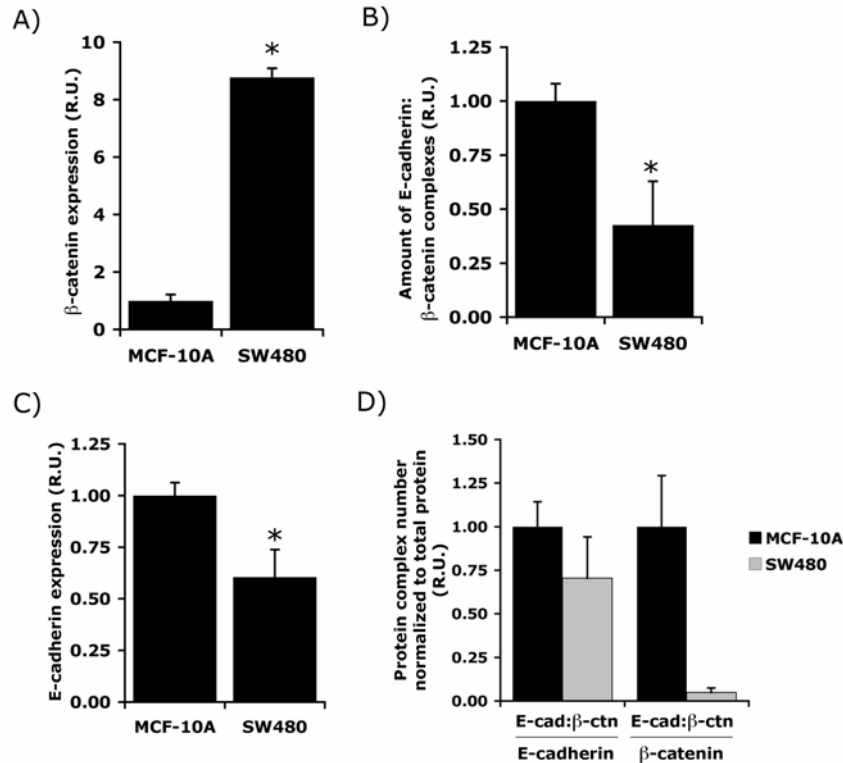
Figure IV-5. Quantitative comparison of the levels of E-cadherin:β-catenin complexes, E-cadherin and β-catenin expression in normal and tumorigenic cell lines.

Whole cell lysates were prepared from MCF-10A and SW480 cells, and were analyzed either by (A) sandwich ELISA for total β-catenin levels, (B) protein complex ELISA for E-cadherin:β-catenin complexes, or (C) sandwich ELISA for total E-cadherin levels. For both the sandwich ELISAs and the protein complex ELISA, the rate of change in optical density over time was plotted versus total cell lysate, as shown in Figure IV-7 (Supplemental Data). The slopes of these curves were normalized to the value of the MCF-10A sample and then reported in relative units (R.U.). Error bars represent 95% confidence intervals on the slope; the asterisk denotes $P < 0.001$, as calculated by ANCOVA. (D) The level of E-cadherin:β-catenin complexes from the protein complex ELISA in MCF-10A and SW480 were normalized to total cellular levels of E-cadherin or β-catenin, as measured by the sandwich ELISA.

To gain more insight into what may be limiting E-cadherin:β-catenin complex formation in SW480 cells, we quantified the E-cadherin expression level in the two cell lines using the sandwich ELISA, revealing that SW480 cells express approximately two-

fold lower levels of E-cadherin per μg of total cell lysate than MCF-10A cells (Figure IV-5C). This two-fold reduction in E-cadherin expression mirrors the two-fold decrease in E-cadherin:β-catenin complexes in SW480 cells, suggesting that the limiting factor in E-cadherin:β-catenin complex formation in SW480 cells is the reduced expression of E-cadherin. In fact, when the levels of E-cadherin:β-catenin are normalized to the total amount of E-cadherin, MCF-10A and SW480 show nearly identical values, with SW480 cells showing only a $30 \pm 24\%$ decrease compared to MCF-10A cells (Figure IV-5D). This suggests that, per E-cadherin molecule, there is no significant difference in binding affinity for β-catenin between the two cell types, although direct measurements are needed to confirm this hypothesis. Thus, the limiting factor in the formation of adherens junctions in SW480 appears to be expression of E-cadherin, especially since SW480 cells express roughly ten-fold higher levels of β-catenin than MCF-10A cells.

To gauge the relative differences in the fraction of cellular β-catenin engaged with E-cadherin between the two cell lines, we normalized the amount of E-cadherin:β-catenin complexes to total levels of β-catenin, as measured by the β-catenin sandwich ELISA. The fraction of cellular β-catenin that is engaged with E-cadherin is approximately 20-fold higher in MCF-10A cells relative to SW480 cells (Figure IV-5D). This result indicates that SW480 possess a much larger pool of β-catenin that is not bound to E-cadherin. Evidently, this arises because SW480 cells express very high levels of total β-catenin with a concomitant decrease in the levels of total E-cadherin, leaving a large fraction of β-catenin unbound to E-cadherin. This pool of unbound β-catenin molecules

may contribute to the constitutive activation of transcriptional targets by β-catenin in SW480.[21]

3.4. Quantitative analysis of the effect of constitutively-active Src on E-cadherin:β-catenin interactions

As another application of our quantitative protein complex ELISA, we quantified the effect of the tyrosine kinase Src on the disruption of adherens junctions in MCF-10A cells, since several lines of evidence have implicated Src in regulating intercellular adhesion.[7, 8, 10, 22] To study the quantitative effects of Src activity on E-cadherin:β-catenin interactions *in vivo* using our protein complex ELISA, MCF-10A cells were infected with retrovirus encoding a constitutively-active mutant of Src (Y527F);[23, 24] as a negative control, cells were infected with retrovirus generated using an empty vector control. Cell lysates were prepared and analyzed for the amount of E-cadherin:β-catenin complexes and for the levels of E-cadherin and β-catenin expression. All assays demonstrated a broad linear range with respect to total cell protein (Supplementary Figure IV-2).

Using the protein complex ELISA revealed that activated Src reduced levels of the E-cadherin:β-catenin complex by ~40% in MCF-10A cells (Figure IV-6A), corroborating reports that Src can disrupt E-cadherin mediated adhesions *in vivo*.[7, 8, 10, 22] These results are consistent with our qualitative observation that sub-confluent MCF-10A cells expressing activated Src formed fewer cell-cell contacts in culture as compared to their empty-vector counterparts (data not shown). To determine whether the reduction in

the amount of E-cadherin:β-catenin complexes correlated with a decrease in E-cadherin:β-catenin interactions or with a decreased expression of these proteins, we quantified the amount of total E-cadherin using the sandwich ELISA. MCF-10A cells expressing activated Src exhibited a reduction in E-cadherin of 40% when compared to cells infected with empty vector control virus (Figure IV-6B). Thus, there is a striking quantitative similarity between the decrease in the levels of E-cadherin:β-catenin complexes and E-cadherin expression. In fact, when the levels of the E-cadherin:β-catenin complex are normalized to total levels of E-cadherin, the ratio is nearly equivalent in cells expressing activated Src and the negative control counterparts (Figure IV-6C).
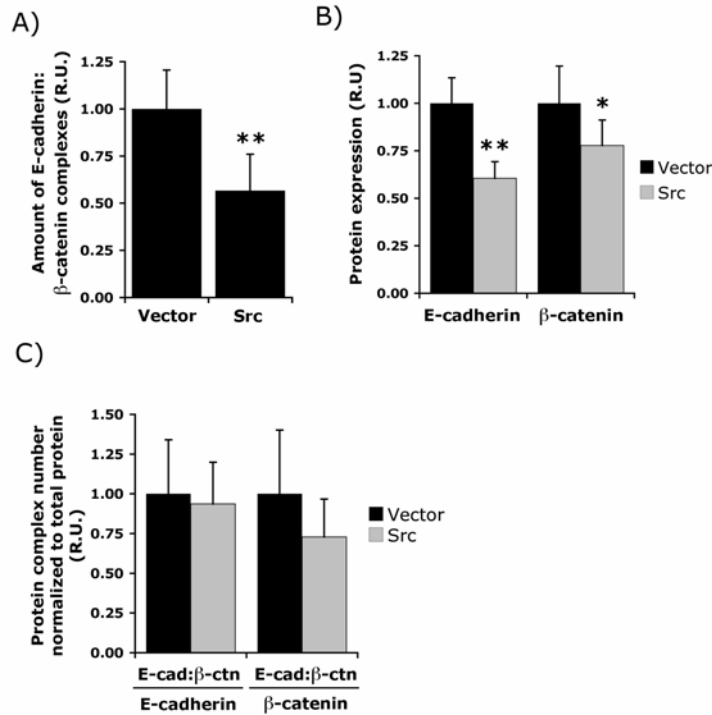
Figure IV-6. Quantifying the effect of constitutively-active Src on cellular levels of E-cadherin:β-catenin complexes and the expression of E-cadherin and β-catenin.

MCF-10A cells were infected with either activated Src (Y527F) or the empty vector control, lysed, and then analyzed either by (A) the E-cadherin:β-catenin ELISA or (B) sandwich ELISAs. For all assays, the rate of change in optical density over time was plotted against total cell lysate, as shown in Figure IV-8 (Supplemental Data). The slopes of these curves were normalized to the value of the empty vector control and then reported in relative units (R.U.). Error bars represent 95% confidence intervals on the slope; the asterisk and double asterisk denote $P < 0.05$ and 0.001, respectively, as calculated by ANCOVA. (D) The level of E-cadherin:β-catenin complexes as measured by the protein complex ELISA was normalized to either total cellular levels of E-cadherin or β-catenin as measured by the sandwich ELISA for both Src-infected and empty vector-infected MCF-10A cells.

Because Src-mediated disruption of adherens junctions *in vivo* correlates with tyrosine phosphorylation of both E-cadherin and β-catenin,[7, 8, 10, 22] it has been speculated that Src disrupts adherens junctions by phosphorylating β-catenin and thus reducing its binding affinity for E-cadherin. In support of this model, *in vitro* studies have

demonstrated that Src-mediated phosphorylation of β-catenin Tyr654 causes a six-fold decrease in the affinity of β-catenin for E-cadherin.[12] Additional *in vitro* studies have also shown that phosphorylation of E-cadherin by Src decreases the affinity constant of E-cadherin for β-catenin from approximately 260 nM to 4 μM *in vitro*.[13]

While our results are not wholly incompatible with this model, the striking correlation between Src-induced decreases in E-cadherin:β-catenin complexes and E-cadherin itself strongly suggests that active Src may reduce the levels of E-cadherin:β-catenin complexes by a simpler mechanism, namely the downregulation of E-cadherin expression. By decreasing the availability of E-cadherin in MCF-10A cells, Src could reduce levels of the endogenous E-cadherin:β-catenin complex without modulating the protein binding affinity through phosphorylation. In another non-transformed epithelial cell line (MDCK), activation of Src induced ubiqutination and endocytosis of E-cadherin through the Hakai ubiquitin ligase, leading to decreased E-cadherin expression and the disruption of cell-cell contacts.[8] Thus, altering the expression level of E-cadherin may be a mechanism by which Src regulates adherens junctions in non-transformed epithelial cells. In fact, Src-mediated downregulation of E-cadherin may contribute to oncogenic phenomena, such as transforming-growth-factor-β-induced epithelial-mesenchymal transition.[25]

The observed 40% decrease in E-cadherin expression raises the question of the fate of its binding partner β-catenin. It is reasonable to hypothesize that a reduction in E-cadherin expression may cause a parallel decrease in β-catenin expression, since when β-

catenin is bound to E-cadherin, it is protected from proteasomal degradation because the degradation complex cannot bind β-catenin.[26] However, once released from E-cadherin, β-catenin is subject to degradation by the APC/axin/GSK3β/casein kinase I degradation machinery. Indeed, the β-catenin ELISA revealed that the expression level of β-catenin also decreased in cells expressing activated Src, but only by a relatively modest 20% (Figure IV-6B). Compared to the 40% reduction in E-cadherin levels, the modest reduction in β-catenin levels suggests that some of the E-cadherin-free β-catenin lingers in the cell, avoiding degradation. Indeed, when the levels of E-cadherin:β-catenin complexes are normalized to total levels of β-catenin, the ratio decreases by ~25% in cells expressing activated Src (Figure IV-6C). This result suggests that among total cellular β-catenin, 25% fewer are associated with E-cadherin in response to constitutive activation of Src, which may contribute to Src-mediated activation of β-catenin-mediated transcription as reported by others.[27, 28]

4. Conclusions

In summary, we have developed a protein complex ELISA to quantify the level of endogenous E-cadherin:β-catenin complexes in unpurified whole cell lysates. Furthermore, we have exploited the compatibility of our protein complex ELISA format to quantify total cellular levels of E-cadherin and β-catenin using traditional sandwich ELISAs. Using these techniques, we have characterized the quantitative differences in E-cadherin:β-catenin complexes between normal and tumorigenic cells as well as the effects of a dominant-active oncogene on E-cadherin:β-catenin complexes *in vivo*. These

measurements provide insight into not only the expression levels of adherens junctions constituents, but also their ability to form multiprotein complexes, which is an integral feature of their biological functionality. Since the association of E-cadherin and β-catenin is an established predictor of tumor cell invasiveness and patient prognosis,[1] the E-cadherin:β-catenin protein complex ELISA may prove to be a powerful tool for diagnostic characterization of tumors. In fact, other protein complex ELISAs have demonstrated that protein complexes can serve as better biomarkers of disease than individual proteins.[14, 16] In addition to the powerful prognostic value of protein:protein association data, the quantitative nature of the protein complex ELISA offers advantages over the qualitative, low-throughput techniques currently used to characterize E-cadherin:β-catenin association. As such, the E-cadherin:β-catenin ELISA is a powerful tool for quantitative characterization of cell-cell adhesion.

5.   Acknowledgements

6.   Materials and Methods

6.1. Cell Culture

MCF-10A cells were cultured in Dulbecco's modified Eagle's medium/Ham's F-12 containing HEPES and L-glutamine (Invitrogen, Carlsbad, CA) supplemented with 5% (v/v) horse serum (Invitrogen), 20 ng/ml EGF (Peprotech, Rocky Hill, NJ), 0.5 µg/ml hydrocortisone (Sigma, Saint Louis, MO), 0.1 µg/ml cholera toxin (Sigma), 10 µg/ml insulin (Sigma), and 1% (v/v) penicillin/streptomycin (Invitrogen). SW480 and 293T cells were cultured in Dulbecco's modified Eagle's medium supplemented with 4 mM L-glutamine (Invitrogen), 10% (v/v) fetal bovine serum (Invitrogen), and 1% (v/v) penicillin/streptomycin (Invitrogen).

6.2. Cell Lysis

Cells were washed twice in ice-cold PBS and scraped into cold modified RIPA buffer (50 mM Tris-Cl (pH 7.5), 150 mM NaCl, 1% (v/v) Triton X-100, 0.5% (v/v) Nonidet P-40, 0.25% (v/v) sodium deoxycholate, 50 mM β-glycerophosphate (pH 7.3), 10 mM NaPP, 30 mM NaF, 1 mM benzamidine, 2 mM EGTA, 1 mM sodium orthovanadate, 1 mM dithiothreitol, 5 µg/ml aprotinin, 5 µg/ml leupeptin, 1 µg/ml pepstatin, and 1 mM phenylmethylsulfonyl fluoride). After incubation on ice for 15 min, the cell lysates were clarified by centrifugation, and the supernatant was collected as whole cell lysate. The protein concentrations were determined using BCA reagents (Sigma, Saint Louis, MO).

6.3. Protein complex and standard ELISAs

Mouse monoclonal capture antibodies against either E-cadherin or β-catenin (BD Transduction Laboratories, San Jose, CA) were diluted to 2.5 μg/ml in Tris-buffered saline (10 mM Tris (pH 8.0), 150 mM NaCl) containing 0.02% (v/v) sodium azide. 100 μl of the diluted capture antibody was then added to a flat-bottom, high-protein-binding 96-well microtiter plate (Corning, Corning, NY) and incubated overnight at room temperature. The next day, the wells were blocked with 150 μl of blocking buffer (10% (v/v) horse serum (Invitrogen, Carlsbad, CA) in TBST (TBS plus 0.05% (v/v) Tween-20) for 2 h at room temperature. After washing the wells three times with TBST, whole cell lysate was diluted in modified RIPA buffer to a final volume of 100 μl and added to each well for 2 h at 37 ºC. The wells were then washed three times with TBST, and 100 μl of either anti-E-cadherin or anti-β-catenin rabbit polyclonal antibody (Santa Cruz Biotechnology, Santa Cruz, CA) diluted to 1 μg/ml in blocking buffer was added to each well and incubated for 1 h at 37 ºC. The wells were washed three times with TBST, and the alkaline phosphatase-conjugated, anti-rabbit IgG secondary antibody (Biosource, Camarillo, CA) was diluted to 1 μg/ml in blocking buffer, and 100 μl was added to each well for 1 h at 37 ºC. For detection, the wells were washed three times with TBST and once with TBS, and then 100 μl of 1 mg/ml *p*-nitrophenyl phosphate (Sigma, Saint Louis, MO) dissolved in reaction buffer (1 M diethanolamine, 0.05 mM $MgCl_2$, pH 9.5) was added to each well. The absorbance at 405 nm was monitored by kinetic read at 37 ºC at 17 second intervals over a period of 22 minutes using a microplate reader (Molecular Devices, Sunnyvale, CA). The rate of change in A405 over time was taken as the assay signal.

For the standard sandwich ELISA, both the capture and the detection antibody targeted the same protein (e.g. monoclonal and polyclonal anti-E-cadherin); for the protein complex ELISAs, the capture and detection antibodies targeted different halves of the E-cadherin:β-catenin protein complex (e.g. monoclonal anti-E-cadherin followed by polyclonal anti-β-catenin).

6.4. Validation of protein capture by Western blotting

Varying amounts of whole cell lysate were incubated in the wells of a microtiter plate that had been coated with either monoclonal anti-E-cadherin or anti-β-catenin antibody and blocked with blocking buffer. After incubation of the whole cell lysate, the plate was washed three times with TBST, and then 100 µl of 1X SDS sample buffer (2% SDS, 0.1 M dithiothreitol, 60 mM Tris (pH 6.8), and 5% (v/v) glycerol diluted in modified RIPA buffer) was added to the wells. The microtiter plate was then incubated for 5 min at 100 $^{\circ}$C, and the contents of the well were collected, resolved by SDS-PAGE on 10% poly-acrylamide gels, and blotted onto nitrocellulose membrane (Bio-Rad, Hercules, CA). The membranes were blocked overnight and then incubated sequentially with primary monoclonal and corresponding horseradish peroxidase-conjugated secondary antibody. The blots were treated with SuperSignal West Femto Substrate (Pierce, Rockford, IL) and imaged on VersaDoc 3000 (Bio-Rad) using Quantity One software (Bio-Rad).

6.5. Plasmid Constructs

pLNCX-Src-Y527F was generously provided by J. Brugge (Harvard Medical School). VSV-G and gag-pol vectors were gifts from D. Schaffer (University of California, Berkeley).

6.6. Retroviral Infection

Retrovirus was produced by triple transfection of 293T cells with 5 μg each of VSV-G, gag-pol and the retroviral vectors pLNCX or pLNCX-Src-Y527F using LipofectAMINE (Invitrogen, Carlsbad, CA) as previously described.[29] For infection, MCF-10A cells were incubated with retrovirus-containing growth medium and 8 μg/ml polybrene (Sigma, Saint Louis, MO) for 24 h; after infection, cells were selected with 200 μg/ml Geneticin (Invitrogen) for 14 days.

6.7. Data Analysis and Statistical Calculations

The Signal/Noise ratio (S/N) was calculated as:

$$S/N = \frac{(\mu_s - \mu_b)}{\sigma_s}$$

where μ_s and μ_b represent the means of the signal and the background, respectively, and σ_s denotes the standard deviation of the assay signal. Z' factors were calculated according to the equation:

$$Z' = 1 - \frac{3 \times (\sigma_s + \sigma_b)}{|\mu_s - \mu_b|}$$

where μ_s, μ_b, and σ_s are as defined above and σ_b is the standard deviation of the blank.[30] The Signal/Noise ratio and the Z' factor were calculated at 200 μg and 130 μg of whole cell lysate for the protein complex ELISAs and the sandwich ELISAs, respectively.

For the studies comparing the expression of E-cadherin, β-catenin, and E-cadherin:β-catenin complexes between cell types (Figure IV-5) or between cells infected with a dominant-active oncogene or an empty vector control (Figure IV-6), linear regressions were performed with total cell protein as the dependent variable and the assay signal (rate of change in optical density at 405 nm over time) as the independent variable, as shown in Figures IV-7 and IV-8 (Supplemental Data). The statistical significance of the observed difference in slopes was calculated by analysis of covariance (ANCOVA).
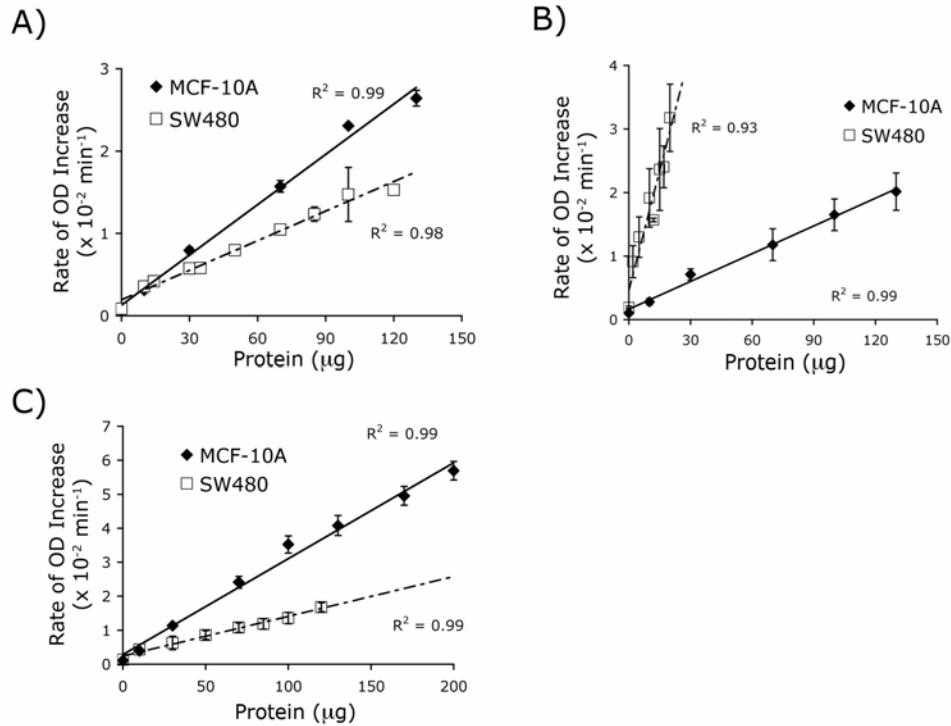
7. Supplemental Data

Figure IV-7. Quantification of E-cadherin, β-catenin, and E-cadherin:β-catenin complexes in normal and tumorigenic cell lines.

Confluent cultures of MCF-10A and SW480 cells were lysed and analyzed by sandwich ELISA for either (A) E-cadherin or (B) β-catenin or by protein complex ELISA for (C) E-cadherin:β-catenin complexes. For all assays, the rate of change in optical density over time was plotted versus total cell lysate, and linear regressions were performed to calculate the slopes of these curves. Error bars represent sample standard error (n=3).
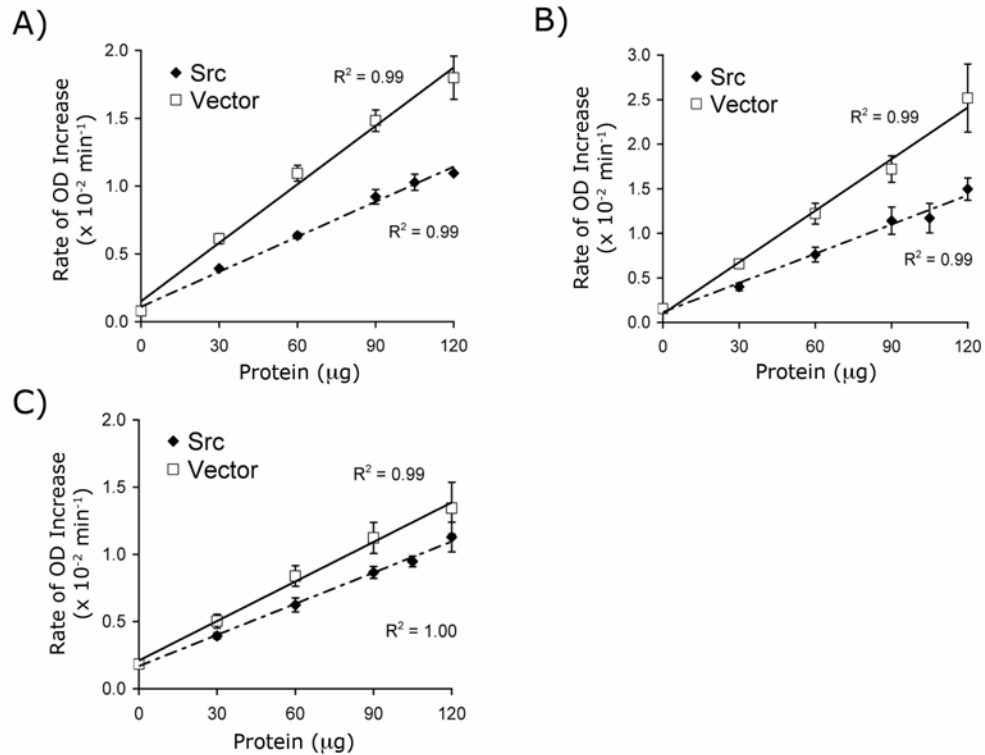
Figure IV-8. Quantifying the effect of constitutively-active Src on cellular levels of E-cadherin:β-catenin complexes and the expression of E-cadherin and β-catenin.

Subconfluent cultures of MCF-10A cells infected with either Src Y527F or the empty vector were lysed and analyzed by sandwich ELISA for (A) E-cadherin or (B) β-catenin expression or by protein complex ELISA for (C) E-cadherin:β-catenin complexes. For all assays, the rate of change in optical density over time was plotted against total cell lysate, and linear regressions were performed to calculate the slopes of these curves. Error bars represent sample standard errors (n = 3).

8. References

1. Wijnhoven BP, Dinjens WN, Pignatelli M. E-cadherin-catenin cell-cell adhesion complex and human cancer. Br J Surg 2000; 87:992-1005.

2. Christofori G, Semb H. The role of cell-adhesion molecule E-cadherin as a tumour suppressor gene. Trends Biochem Sci 1999; 24:73-6.

3. Angst BD, Marcozzi C, Magee AI. The cadherin superfamily. J Cell Sci 2001; 114:625-6.

4. Hirohashi S. Inactivation of the E-cadherin-mediated cell adhesion system in human cancers. Am J Pathol 1998; 153:333-9.

5. De Leeuw WJ, Berx G, Vos CB, Peterse JL, Van de Vijver MJ, Litvinov S, Van Roy F, Cornelisse CJ, Cleton-Jansen AM. Simultaneous loss of E-cadherin and catenins in invasive lobular breast cancer and lobular carcinoma in situ. J Pathol 1997; 183:404-11.

6. Ohene-Abuakwa Y, Noda M, Perenyi M, Kobayashi N, Kashima K, Hattori T, Pignatelli M. Expression of the E-cadherin/catenin (α-, β-, and γ-) complex correlates with the macroscopic appearance of early gastric cancer. J Pathol 2000; 192:433-9.

7. Behrens J, Vakaet L, Friis R, Winterhager E, Van Roy F, Mareel MM, Birchmeier W. Loss of epithelial differentiation and gain of invasiveness correlates with tyrosine phosphorylation of the E-cadherin/β-catenin complex in cells transformed with a temperature-sensitive v-SRC gene. J Cell Biol 1993; 120:757-66.

8. Fujita Y, Krause G, Scheffner M, Zechner D, Leddy HE, Behrens J, Sommer T, Birchmeier W. Hakai, a c-Cbl-like protein, ubiquitinates and induces endocytosis of the E-cadherin complex. Nat Cell Biol 2002; 4:222-31.

9. Lu Z, Ghosh S, Wang Z, Hunter T. Downregulation of caveolin-1 function by EGF leads to the loss of E-cadherin, increased transcriptional activity of β-catenin, and enhanced tumor cell invasion. Cancer Cell 2003; 4:499-515.

10. Avizienyte E, Wyke AW, Jones RJ, McLean GW, Westhoff MA, Brunton VG, Frame MC. Src-induced de-regulation of E-cadherin in colon cancer cells requires integrin signalling. Nat Cell Biol 2002; 4:632-8.

11. Gottardi CJ, Gumbiner BM. Distinct molecular forms of β-catenin are targeted to adhesive or transcriptional complexes. J Cell Biol 2004; 167:339-49.

12. Roura S, Miravet S, Piedra J, Garcia de Herreros A, Dunach M. Regulation of E-cadherin/catenin association by tyrosine phosphorylation. J Biol Chem 1999; 274:36734-40.

13. Catimel B, Layton M, Church N, Ross J, Condron M, Faux M, Simpson RJ, Burgess AW, Nice EC. *In situ* phosphorylation of immobilized receptors on biosensor surfaces: application to E-cadherin/β-catenin interactions. Anal Biochem 2006; 357:277-88.

14. Wang J, Qiang H, Zhang C, Liu X, Chen D, Wang S. Detection of IgG-bound lipoprotein(a) immune complexes in patients with coronary heart disease. Clin Chim Acta 2003; 327:115-22.

15. Strandberg K, Kjellberg M, Knebel R, Lilja H, Stenflo J. A sensitive immunochemical assay for measuring the concentration of the activated protein

C-protein C inhibitor complex in plasma: use of a catcher antibody specific for the complexed/cleaved form of the inhibitor. Thromb Haemost 2001; 86:604-10.

16. Ogasawara K, Mashiba S, Wada Y, Sahara M, Uchida K, Aizawa T, Kodama T. A serum myloid A and LDL complex as a new prognostic marker in stable coronary artery disease. Atherosclerosis 2004; 174:349-56.

17. Harris TJ, Peifer M. Decisions, decisions: β-catenin chooses between adhesion and transcription. Trends Cell Biol 2005; 15:234-7.

18. Butler JE, Navarro P, Sun J. Adsorption-induced antigenic changes and their significance in ELISA and immunological disorders. Immunol Invest 1997; 26:39-54.

19. Tait L, Soule HD, Russo J. Ultrastructural and immunocytochemical characterization of an immortalized human breast epithelial cell line, MCF-10. Cancer Res 1990; 50:6087-94.

20. Munemitsu S, Albert I, Souza B, Rubinfeld B, Polakis P. Regulation of intracellular ®-catenin levels by the adenomatous polyposis coli (APC) tumor-suppressor protein. Proc Natl Acad Sci U S A 1995; 92:3046-50.

21. Korinek V, Barker N, Morin PJ, van Wichen D, de Weger R, Kinzler KW, Vogelstein B, Clevers H. Constitutive transcriptional activation by a ®-catenin-Tcf complex in APC^{-/-} colon carcinoma. Science 1997; 275:1784-7.

22. Owens DW, McLean GW, Wyke AW, Paraskeva C, Parkinson EK, Frame MC, Brunton VG. The Catalytic Activity of the Src Family Kinases is Required to Disrupt Cadherin-dependent Cell-Cell Contacts. Mol Biol Cell 2000; 11:51-64.

23. Piwnica-Worms H, Saunders KB, Roberts TM, Smith AE, Cheng SH. Tyrosine phosphorylation regulates the biochemical and biological properties of pp60c-src. Cell 1987; 49:75-82.

24. Cartwright CA, Eckhart W, Simon S, Kaplan PL. Cell transformation by pp60c-src mutated in the carboxy-terminal regulatory domain. Cell 1987; 49:83-91.

25. Galliher AJ, Schiemann WP. β3 Integrin and Src facilitate transforming growth factor-beta mediated induction of epithelial-mesenchymal transition in mammary epithelial cells. Breast Cancer Res 2006; 8:R42.

26. Hulsken J, Birchmeier W, Behrens J. E-cadherin and APC compete for the interaction with β-catenin and the cytoskeleton. J Cell Biol 1994; 127:2061-9.

27. Ress A, Moelling K. Bcr interferes with β-catenin-Tcf1 interaction. FEBS Lett 2006; 580:1227-30.

28. Haraguchi K, Nishida A, Ishidate T, Akiyama T. Activation of β-catenin-TCF-mediated transcription by non-receptor tyrosine kinase v-Src. Biochem Biophys Res Commun 2004; 313:841-4.

29. Kim VN, Mitrophanous K, Kingsman SM, Kingsman AJ. Minimal requirement for a lentivirus vector based on human immunodeficiency virus type 1. J Virol 1998; 72:811-6.

30. Zhang JH, Chung TD, Oldenburg KR. A Simple Statistical Parameter for Use in Evaluation and Validation of High Throughput Screening Assays. J Biomol Screen 1999; 4:67-73.